Summer 9-30-1971

The oxidation of carbon monoxide by magnesium aluminate

James A. Whelan
New Jersey Institute of Technology

Copyright Warning & Restrictions

The copyright law of the United States (Title 17, United States Code) governs the making of photocopies or other reproductions of copyrighted material.

Under certain conditions specified in the law, libraries and archives are authorized to furnish a photocopy or other reproduction. One of these specified conditions is that the photocopy or reproduction is not to be "used for any purpose other than private study, scholarship, or research." If a, user makes a request for, or later uses, a photocopy or reproduction for purposes in excess of "fair use" that user may be liable for copyright infringement,

This institution reserves the right to refuse to accept a copying order if, in its judgment, fulfillment of the order would involve violation of copyright law.

Please Note: The author retains the copyright while the New Jersey Institute of Technology reserves the right to distribute this thesis or dissertation

Printing note: If you do not wish to print this page, then select "Pages from: first page # to: last page #" on the print dialog screen

INFORMATION TO USERS

This dissertation was produced from a microfilm copy of the original document. While the most advanced technological means to photograph and reproduce this document have been used, the quality is heavily dependent upon the quality of the original submitted.

The following explanation of techniques is provided to help you understand markings or patterns which may appear on this reproduction.

1. The sign or "target" for pages apparently lacking from the document photographed is "Missing Page(s)". If it was possible to obtain the missing page(s) or section, they are spliced into the film along with adjacent pages. This may have necessitated cutting thru an image and duplicating adjacent pages to insure you complete continuity.

2. When an image on the film is obliterated with a large round black mark, it is an indication that the photographer suspected that the copy may have moved during exposure and thus cause a blurred image. You will find a good image of the page in the adjacent frame.

3. When a map, drawing or chart, etc., was part of the material being photographed the photographer followed a definite method in "sectioning" the material. It is customary to begin photoing at the upper left hand corner of a large sheet and to continue photoing from left to right in equal sections with a small overlap. If necessary, sectioning is continued again — beginning below the first row and continuing on until complete.

4. The majority of users indicate that the textual content is of greatest value, however, a somewhat higher quality reproduction could be made from "photographs" if essential to the understanding of the dissertation. Silver prints of "photographs" may be ordered at additional charge by writing the Order Department, giving the catalog number, title, author and specific pages you wish reproduced.

University Microfilms

300 North Zeeb Road
Ann Arbor, Michigan 48106

A Xerox Education Company

THE OXIDATION OF CARBON MONOXIDE BY MAGNESIUM ALUMINATE

BY

JAMES A. WHELAN

A DISSERTATION

PRESENTED IN PARTIAL FULFILLMENT OF

THE REQUIREMENTS FOR THE DEGREE

OF

DOCTOR OF ENGINEERING SCIENCE IN CHEMICAL ENGINEERING

AT

NEWARK COLLEGE OF ENGINEERING

Newark, New Jersey

1971

ABSTRACT

In this research the catalytic oxidation of carbon monoxide was investigated on magnesium aluminate catalysts, $MgO:xAl_2O_3$, with five different compositions, x, ranging from 1.0 to 3.0. The reaction was run at temperatures ranging from 500 to 600 ^{o}C. with radioactive carbon monoxide as the tracer. An experimental technique has been devised for the analysis of unreacted CO which takes into account a correction for the solubility of CO in CO_2.

Four mathematical models were postulated to explain the mechanism of reaction. The models were examined against experimental data by means of non-linear least squares analysis. One model was found to fit the experimental data substantially better than the other models. This model is considered to represent a plausible explanation for the results of this study.

From the mathematical modeling it was found that the oxidation reaction proceeds by the reaction of gaseous CO with chemisorbed oxygen. The chemisorption involved in the process is of the "weak" type; oxygen is chemisorbed as a boundary layer and not by transfer of electrons. The importance of the electronic properties of a catalyst are called into question in this work because of the fact that magnesium aluminate is an insulator.

It is found that the activation energy and the number of active sites reaches a maximum at an Al_2O_3/MgO ratio equal to 1.667.

The catalytic activity is not directly related to the number of cation vacancies. The active sites for "weak" oxygen adsorption are the normal aluminum lattice cations, located in octahedral positions of the spinel structure.

The composition of crystal mixture in a single crystal structure is one of the factors which will greatly affect catalytic activity. The observed compensation effect of catalytic activity is related to the catalyst composition; the catalyst composition affects the strength of adsorption bond between the catalyst and adsorbed oxygen and also the number of pre-precipitation nuclei. The former affects the activation energy; the latter affects the number of active sites.

APPROVAL OF DISSERTATION

THE OXIDATION OF CARBON MONOXIDE

BY MAGNESIUM ALUMINATE

BY

JAMES A. WHELAN

FOR

DEPARTMENT OF CHEMICAL ENGINEERING

NEWARK COLLEGE OF ENGINEERING

BY

FACULTY COMMITTEE

APPROVED: _____ Chairman

_____

_____

_____

_____

NEWARK, NEW JERSEY

SEPTEMBER, 1971

ACKNOWLEDGMENTS

The author would like to express his sincere graditude and appreciation to the following persons and organizations for their assistance and support in his work:

Dr. Ching-Rong Huang , thesis advisor - for his guidance and encouragement in all phases of this work.

Dr. C.C. Wang, RCA Laboratories, Princeton, New Jersey --for information regarding magnesium aluminate.

RCA Laboratories, Princeton, New Jersey -- for supplying samples of magnesium aluminate.

Newark College of Engineering -- for financial support for three years as a teaching fellow.

NDEA --for financial support for one year.

TABLE OF CONTENTS

LIST OF FIGURES

LIST OF FIGURES

CHAPTER I

INTRODUCTION

Since 1900, catalysis has become the major route to chemical transformation in most of the chemical process industries. Catalysis has had a multiplying effect in the productivity of basic chemicals. It has sparked the advent of previously unknown products and has stimulated the establishment of new industries. The 1962 wholesale value of products resulting from heterogeneous catalytic processes amounted to about $19,500,000,000 - or about 15% of the $130 billion total of all manufactured goods.(1)

The classic definition of catalysis(2) is that a catalyst is any substance that alters the rate of a chemical reaction without itself being altered by the resultant reaction. It is now generally agreed(3) that the catalyst actually is altered during reaction, but its original state is continuously regenerated. The catalyst, in effect, provides the chemical reactants with an alternate route to reaction in which the energy of activation is much lower.

The purpose of this research was to study the catalytic activity of magnesium aluminate as a function of its composition. The reaction chosen to study the

catalytic activity was the oxidation of carbon monoxide. Since carbon monoxide is one of the major pollutants of the atmosphere, it was anticipated that a fundamental study of surface reactions might contribute to the control of carbon monoxide propagation to the atmosphere.

The majority of studies in the literature attempting a theoretical understanding of catalysis have employed semiconductor or metal catalysts. An elaborate and complicated theory, known as the Electronic Theory of Catalysis, was developed during the decade of the 1950's.[4] In essence, this theory attempts to relate a correlation between the electronic properties of a catalyst and its catalytic activity. Implicit in this theory is the idea that catalysis evolves principally through electronic charge transfer between adsorbate and adsorbent as a whole. The Electronic Theory of Catalysis successfully explained a wide range of catalytic reactions; however, many inconsistencies of the theory in accounting for some reactions did not allow for a complete acceptance of the theory.[5] Examples of these inconsistencies will be presented.

The only other theory of importance has been Balandin's Multiplet Theory.[86] The essence of Balandin's theory is that the activity of a catalyst depends to a large degree on the presence in the lattice of correctly spaced groups (or multiplets) of atoms to accommodate the various reactant molecules to form products. There has been both experimental

confirmation and dispute regarding the validity of this theory.[2] The theory has been applied to catalysts of simple cubic structure; for the present work with spinels, which present a much more complex structure than simple cubic structures, the present state of development of Balandin's theory offers no help.

Magnesium aluminate, $MgO:xAl_2O_3$, was chosen as the catalyst for the following six reasons:

(1) Magnesium aluminate is classified as an insulator. If it could be shown that the catalytic activity of an insulator varies with its composition, this would suggest that there must be effects other than the electronic charge transfer between adsorbate and adsorbent contributing to the catalytic activity, since electrical conductivity is negligible in an insulator.

(2) In Al-rich spinels ($MgO:xAl_2O_3$, $x > 1.0$) the aluminum excess causes atomic defects in the form of vacancies in the spinel lattice; the vacancies are a direct function of the Al to Mg ratio in the lattice. This is shown in Figure 5, p. 22. By changing the Al to Mg ratio the need for the use of impurities in the crystal lattice to study the catalytic activity is eliminated. The use of impurities to vary electrical properties in the catalyst would create the possibility of distorting the crystal structure. Hence the importance of vacancies to catalytic

activity may be investigated.

(3) Magnesium aluminate is chemically stable up to 1200 °C in the atmosphere due to its close-packed, face-centered cubic arrangement of the spinel structure. With composition, x, ranging from .64 to 6.7, the spinel is found stable in one phase.[6]

(4) The crystal structure and physical properties of magnesium aluminate have been investigated extensively.

(5) Stoichiometric magnesium aluminate used in this study was specially prepared (by RCA) by a flux technique developed by RCA Laboratories.[7] Non-stoichiometric spinel was prepared at RCA by a flame-fusion technique.[8] These methods of preparing single crystals produce crystals which contain many fewer defects than commercially prepared spinels.[9] Samples of these RCA crystals were made available for this study.

(6) An important feature of the RCA samples is that they are reproducible. Reproducibility has been achieved by close control of the feed preparation and of the growth conditions.[6]

CHAPTER II

PREVIOUS INVESTIGATIONS

A. The Catalytic Oxidation of Carbon Monoxide.

The catalytic oxidation of carbon monoxide (COCM) has played an important role in the development of understanding of heterogeneous catalysis. A careful and assiduous study of surface reactions involving carbon monoxide has led to a better understanding of the role which the catalyst plays.

The majority of catalysts studied in the COCM have been semiconductor catalysts. Semiconductor theory had been well developed in the 1950's and the electron and hole transport in semiconductors was explained remarkedly well by the band theory of solids.[10] Attempts to correlate the electronic properties of semiconductors with their catalytic activity met with a moderate degree of success. However, as stated by Wolkenstein:[4] "The results of the electron theory as developed for semiconductors...cannot ...be automatically applied to metals. The application of the band theory of solids to metals cannot be considered as well justified at the present time. This is especially true for the transition metals and for chemical processess on metal surfaces." Hence, semiconductor

catalysts are preferrable to metal catalysts in theoretical studies of catalysis at the present time. Semiconductors are also particularly attractive for study as catalysts because their behavior and reactions with electrons can be treated by the well known methods of classical physical chemistry, e.g., by the Boltzmann statistics.

Schwab and Block[11] correlated the electronic properties of nickel oxide and its catalytic activity. Since nickel oxide occurs naturally as a p-type semiconductor, the addition of monovalent cations such as lithium would increase the conductivity. The addition of trivalent ions such as the cations of chromium should decrease the number of positive holes, and hence decrease the conductivity.

The work of Hauffe and Verwey[12] illustrates (see Figure 1) the influence of these added alter ions. Figure 1 also shows the results of Schwab and Block for the catalytic oxidation of carbon monoxide. The addition of lithium oxide increases the conductivity of nickel oxide and lowers the energy of activation for carbon monoxide in the temperature range of 300 to 450 °C. Addition of trivalent chromium ions lowers the conductivity and raises the energy of activation for the catalytic reaction. Schwab and Block concluded that the

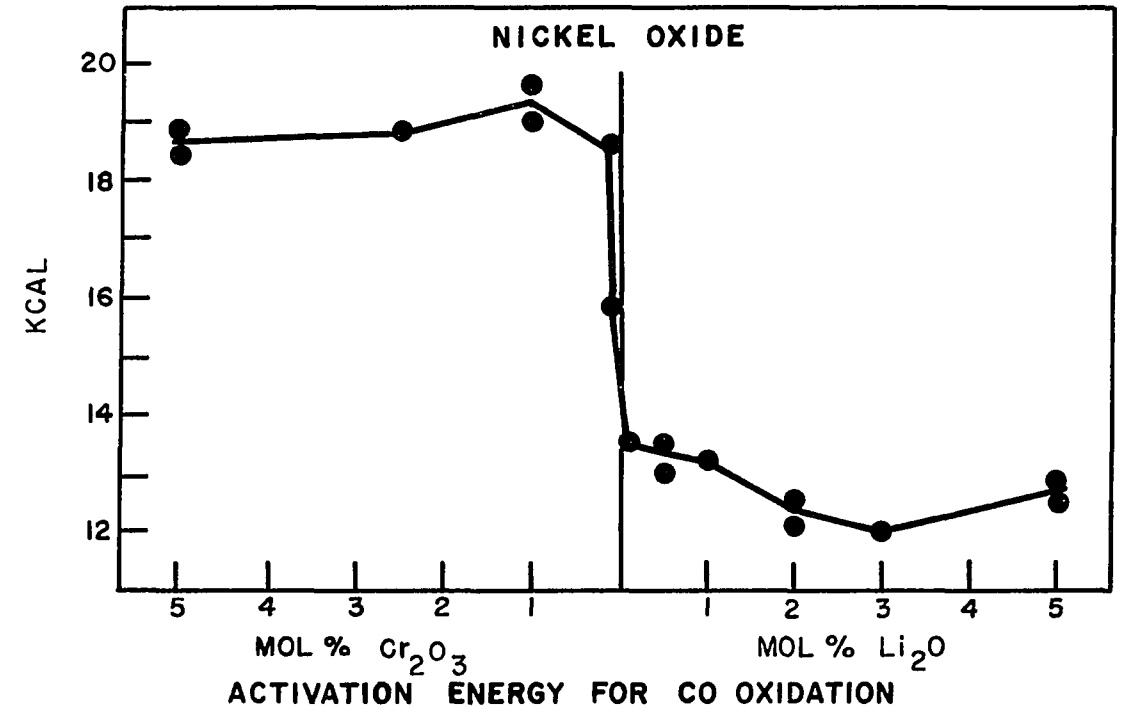

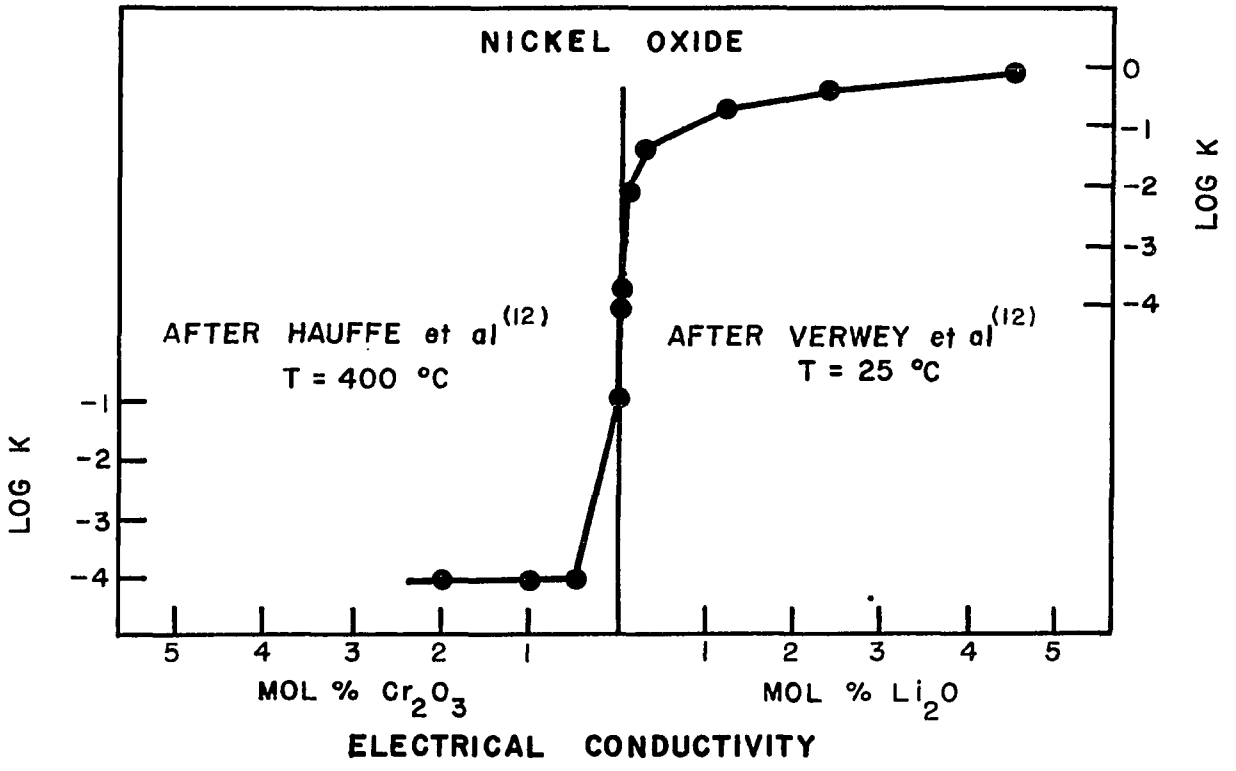

Figure 1 Activation energy for the catalytic oxidation of carbon monoxide and electrical conductivity for NiO doped oxides of chromium or lithium. From Schwab.[11]

rate determining step in the oxidation of carbon monoxide is the formation of positive ions on the surface of p-type semiconductor nickel oxide. This is justified by the rate of oxidation over nickel oxide which is proportional to the first power of carbon monoxide pressure.

The work of Schwab and Block was called into question by the work of Parravano.[13] Parravano found that the energy of activation for the COCM over nickel oxide increased rather than decreased as lithium oxide was added to the nickel oxide. The addition of trivalent chromium oxide caused a lowering of the energy of activation rather than an increase.

There are two important reasons for the discrepancies in these two works.[87] Parravano used lower concentrations of dopents in his studies. This suggests that the crystal properties may have been different in Parravano's work. The second reason for the different results of the two works was the lower temperature range in which Parravano worked - the reaction was carried out in the range 180 to 250 °C., as compared to a temperature range of 250 to 450 °C. used by Schwab and Block.

The work of Parravano has been confirmed by Keier, Roginskii and Sozonova[14] and also by Cimino, Molinari and Romeo.[15] The work of Schwab and Block has been confirmed by Dry and Stone,[16] and also by Komatsu, Ooki, Naki and Kobayashi.[17]

Parravano concluded that during the oxidation of carbon monoxide on pure nickel oxide in the temperature range 160 to 222 °C the concentration of excess oxygen in the solid phase is paramount in determining the type of kinetics followed by the oxidation reaction.[18]

Roginskii and Tselinskaya[19] found nickel oxide to be a catalyst for the carbon monoxide oxidation at room temperature, though the surface gradually becomes self-poisoned by carbon dioxide adsorption. These authors reported that poisoning was absent at temperatures above 160-200 °C.

These findings of Roginskii and Tselinskaya were confirmed by Dell and Stone.[20] Taking the heat of desorption of carbon dioxide at 28 kcal/mole (numerically equal to the heat of adsorption which is usual for CO_2), the time required for half-desorption is 5×10^6 seconds at 20 °C., but only 5 seconds at 150 °C. Poisoning can therefore be expected at 20 °C but should be absent above about 150 °C. In addition, CO_3^- complex will form on some sites and since this is stable to CO at 20 °C it will also act as a poison.

Both Schwab and Block and Parravano reported initial fluctuations in rate data until steady state activity of catalyst was reached. Eaton and Winter[21] studied surface

area changes of nickel oxide catalysts during carbon monoxide oxidation at 2 and 20 cm. Hg. pressure. These investigators reported substantial changes in the BET areas of nickel oxide and lithium oxide doped nickel oxide catalysts. Eaton and Winter suggested that exchange of oxygen betweeen particularly active sets of surface sites and the oxygen-containing gases will,during many repeated experiments, produce a gradual rearrangement of the surface which will be influenced by, and will itself influence, underlying defects. An array of a large number of subsurface lattice defects, such as occurs along borders of microdomains, or at slip planes or screw dislocations, etc., might by this means be "unlocked", leading to a considerable increase in the surface area available to gas molecules. Eaton and Winter also hypothesized that it is possible that the change in mechanism of the COCM which is thought to occur around 250 ^{o}C. on nickel oxide is due to a change in the nature of the chemisorbed oxygen from mainly charged molecular oxygen, O_2^- at low temperatures to atomic oxygen, O^- above 250 ^{o}C.; this is in part confirmed by a change in the kinetics of O_2 adsorption at this temperature.

El Shobaky, Gravelle and Teichner[22] studied the COCM at 30 ^{o}C. on pure and NiO doped with lithium and gallium. They concluded that the catalyst

activity is related to the surface defect structure and to the energy distribution of the surface adsorption sites rather than to the electronic structure of the catalysts. The nickel oxide was prepared by dehydration of the hydroxide under vacuum ($p = 10^{-6}$ torr) at 200 °C.

In another paper, El Shobaky, Gravelle and Teichner[23] repeated the experiment but prepared the nickel oxide at 250 °C. They reached the same conclusion as in the previous paper, and they also noted a greater catalytic activity for the oxide prepared at 250 °C., even though the electrical properties of both oxides were identical. They attributed the greater activity of the oxide prepared at 250 °C. to the difference in the reactivity of oxygen adsorbed on both surfaces.

Matsuura et al[24] expressed the opinion that both dopents of tri and uni-valent ions did not effect essentially the activation energy and that the slight difference of the energy caused by the dopents should be ascribed to the different degree of poisoning of the catalyst by carbon dioxide.

Komatsu, Ooki, Naka and Kobayashi[25] studied the catalytic activity of mixtures of nickel oxide with different dopents in the COCM. The activity of mixtures increased to several times greater than would be predicted by a simple additive effect of single doped catalyst. These authors postulated a mechanism to explain the

enhanced activity of catalyst mixtures.

One such mixture studied was that of NiO-Li_2O and NiO-In_2O_3. When the two oxides are brought into contact in a reactor, an electron rearrangement occurs in such a way as to equalize Fermi levels at the interface, exhibiting a positive and negative space charge in the indium doped oxide and in the lithium doped oxide, respectively. Direct or indirect contact between the two oxides is assumed. The positive charge on the indium doped oxide favors the chemisorption of carbon monoxide as CO^+_{ads} and the amount of CO^+_{ads} on the indium doped oxide may be greater than on the single oxide which has no positive charge and is neutral. The negative charge on the lithium doped oxide favors the chemisorption of oxygen as O^-_{ads} and the amount of O^-_{ads} on the lithium doped oxide is also greater than on the single oxide. The CO^+_{ads} ions may diffuse through the contact zone from one component of the catalyst to the other and react to form CO_2, neutralizing the space charge. When the neutralization of space charge takes place, the positive and negative charges are again regenerated on the two oxides.

Schwab and Block[26] studied the oxidation of carbon monoxide over zinc oxide. Since zinc oxide occurs naturally as an n-type semiconductor, the addition of

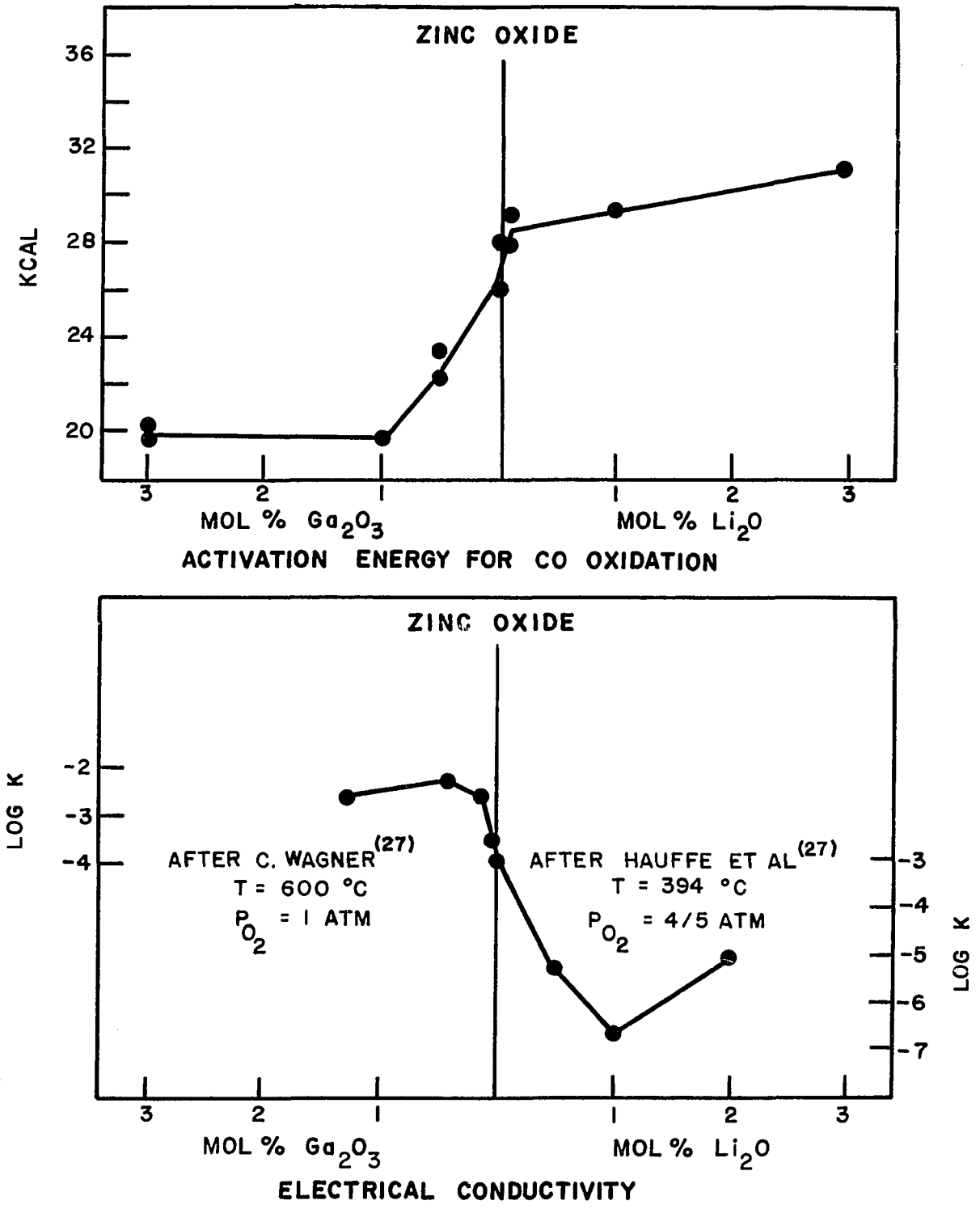

Figure 2. Activation energy for the catalytic oxidation of carbon monoxide and electrical conductivity for ZnO doped with oxides of gallium or lithium. From Schwab.[11]

monovalent lithium ions decreases the number of free electrons and decreases the conductivity of the semiconductor. The addition of trivalent gallium ions increases the conductivity by increasing the supply of free electrons. This is illustrated in Figure 2, from the work of Wagner and Hauffe.[27] The energy of activation increases as the concentration of lithium increases. The increase in concentration of trivalent gallium ions causes a marked decrease in the energy of activation. Schwab concluded that the COCM over zinc oxide involves the chemisorption of oxygen as the slow step. Since oxygen is an electron acceptor, the greater the supply of electrons at the surface of the zinc oxide semiconductor, the easier will be the formation of the surface oxygen ions, and hence the lower the energy of activation for the catalytic reaction. This hypothesis was justified by kinetics, which indicates that the slow step in the reaction is the rate of chemisorption of oxygen.

Chon and Prater[28] used the Hall effect to study the COCM over zinc oxide and concluded that O^- is the dominant, but probably not the only, reactive species in a reaction with electron transfer to the ZnO in the temperature range of 200 to 350 ^{o}C.

Amigues and Teichner[29] observed that the reaction

between CO and O_2 at 261 °C produced in ZnO a slow increase of the electrical conductivity (half time τ of electron transfer reaction 10 to 70 min.), and they concluded that a nonionic oxygen species reacts with CO. These large values of τ are probably due to the large residual oxygen pressure that these investigators used. That is, until the partial pressure of oxygen is reduced by the CO reaction, the electrons of the bulk will tend to be localized on sorbed oxygen species.

Sancier[30] concluded from electron spin resonance studies that CO reacts on ZnO catalysts with two sorbed oxygen species, probably O_2^- and O^-.

Hoang-Van and Teichner[31] studied the COCM on amorphous aluminas; these investigators found that the catalytic activity is determined by surface defects consisting of oxygen or aluminum ion vacancies. Having degassed the alumina at a pressure of 10^{-6} torr, in the temperature range 450-700 °C., the catalytic activity and the concentration of oxygen vacancies pass through a maximum at 500-550 °C. Degassing the alumina above 700 °C. causes the catalytic activity to increase again, apparently because of a marked increase in the number of aluminum cation vacancies. The rate of the COCM at 500 °C. on degassed alumina is first order with respect to oxygen and carbon monoxide concentration, indicating weak

adsorption of both oxygen and carbon monoxide on this surface. Oxygen preatment at 500 °C. of alumina previously degassed at 500 °C. negated the activating effect of the degassing, owing to the filling of oxygen vacancies. Treatment of the alumina with carbon monoxide at 500 °C. leads to an increase in the concentration of oxygen vacancies and a corresponding increase in catalytic activity. CO pretreatment may form new types of active sites in addition to those activated in vacuo. Greater unsaturation of oxygen sites caused by CO pretreatment leads to stronger adsorption of both carbon monoxide and oxygen during catalytic oxidation, as evidenced by the fact that the kinetic orders with respect to oxygen and carbon monoxide become nearly zero. This work points out emphatically that the predominant type of surface defect and its concentration depends on the conditions of pretreatment of the catalyst prior to catalysis.

This brief survey of the COCM should serve to point out the many variables and uncertainties one deals with in catalytic reactions. Discussion of theories of catalytic reactions <u>in general</u> is profitless, if not illusory, because the methods of operation of catalysts are as varied as the modes of chemical change. This survey of the COCM is by no means exhaustive - more extensive reviews of the investigation of this reaction are available.(32)

To date there have been no studies reported in the

literature of the COCM on magnesium alulmnate, nor is there any report of the effect of the composition of solid mixture upon the catalytic activity of an insulator.

B. Properties of Magnesium Aluminate.

The magnesium aluminate system represents a large class of oxides having the general formula AB_2O_4 which crystallize with the crystal structure called spinel. The "ideal" crystal structure of spinel was determined in 1915.[33] The spinel structure is characterized by face-centered cubic close packing of O^{-2} ions and A^{+2} and B^{+3} metallic ions in certain interstices. The distribution of cations in the structure of non-stoichiometric spinel is not well understood. A unit cell and the atomic positions in the spinel structure is shown in Figures 3 and 4. There are eight $MgAl_2O_4$ units per cell, if the magnesium aluminate is stoichiometric. Among the 24 cation sites, eight of them, the tetrahedral sites (coordination number 4), are tetrahedrally coordinated by oxygen. The remaining 16 sites, the octahedral sites (coordination number 6), are octahedrally coordinated by oxygen. The distribution of metal ions and vacancies in the tetrahedral and octahedral cation sites depends on the site preference energies, which vary with composition and, probably, the thermal history of the material. The structure is further complicated by the distribution of

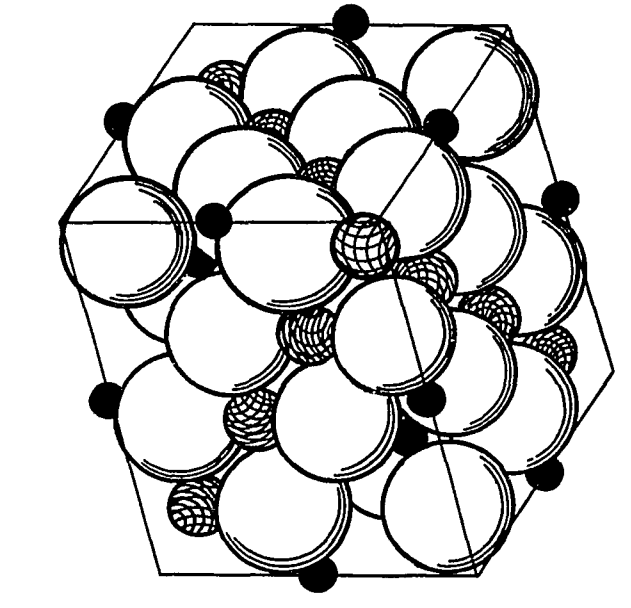

● TETRAHEDRAL SITE (88% Mg + 12% Al)

OCTAHEDRAL SITE (6% Mg + 94% Al

○ OXYGEN

FIGURE 3. UNIT CELL OF $MgAl_2O_4$.[6]

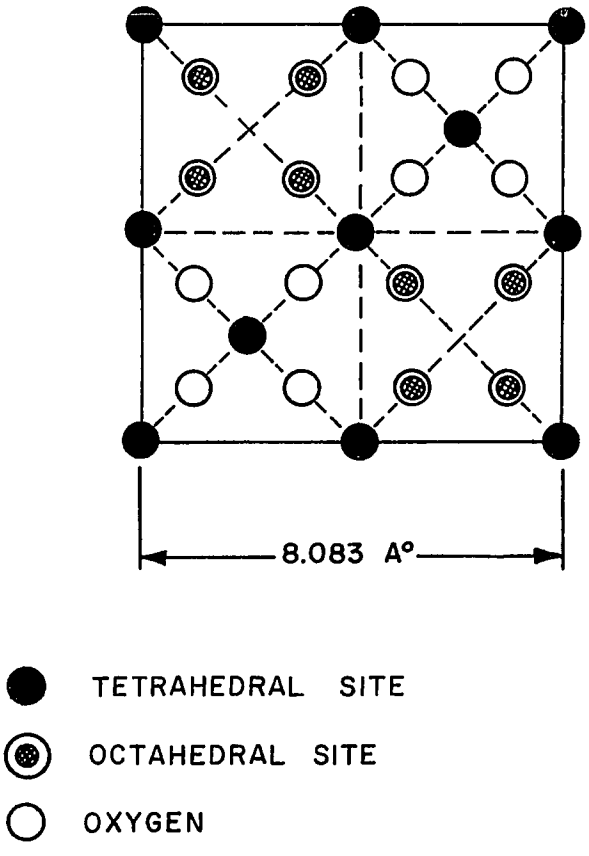

FIGURE 4. PLANE PROJECTION OF HALF A UNIT CELL OF $MgAl_2O_4$ SPINEL.[6]

vacancies and ions[34], by inverson of ions[35], by composition variation[36], by charge compensation requirements[37], by precipitation phenomena and pre-precipitation phenomena[36], and by local structural reorganization.[37]

The "normal" form of spinel, $Mg(Al_2)O_4$ occurs with stoichiometric spinel. The Mg^{+2} ions occupy the tetrahedral sites and the Al^{+3} ions occupy the octahedral sites. The true structure of spinel is more likely the "inverse" spinel, $Mg_xAl_{1-x}(Mg_{1-x}Al_{1+x})O_4$. In inverse spinel the sixteen octahedral sites are occupied half by A^{+2} and half by B^{+3}. The exact degree of inversion (1-x) is not known; an approximate value is 12%. For the Al-rich spinel, the degree of inversion is further influenced by the presence of vacancies and is also not known.

Magnesium aluminate is an insulator. Its dielectric conductivity, C, is given by

$$C = 5.5 \times 10^{11} \cdot f \cdot k \cdot \tan \delta \qquad \text{(in ohm-cm.)}^{-1}$$

where f is frequency, k is dielectric constant, and tan δ is the dissipation factor. The dependence of K and tan δ on Mg/Al ratio in spinel is minimal - not noticeable within range of experimental error.[85]

C. Composition of Magnesium Aluminate.

Solid mixtures of magnesium aluminate can be made with an unusually wide range of composition which extends from approximately $MgO:0.6Al_2O_3$ to $MgO:6.7Al_2O_3$. The vacancies, $\square$, may be written in the structural formula in the form

$(MgAl_2O_4)_1 \cdot (Al_{8/3}\square_{1/3}O_4)_{3(x-1)/4}$.

In Al-rich spinel, the aluminum excess in the spinel lattice is accompanied by vacancies in the metal position. Based on the assumption that the Al-rich spinel is a solid solution of $MgAl_2O_4$ and Al_2O_3, the vacancy is a direct function of the Al to Mg ratio in the lattice. This is shown in Figure 5. The vacancies are atomic defects. Commercial spinel, conventionally prepared by flame fusion, is aluminum rich and has a composition of about $MgO:3.3Al_2O_3$. This is the most easily prepared composition. Little is known about the Mg-rich spinel, and the excess Mg ions may be present as interstitial ions.

D. Method of Crystal Preparation.

The spinel crystals used in this research were obtained from RCA Laboratories, Princeton, New Jersey. RCA has developed a crystal growth technique for low Al-rich ($1.5<x<2.5$) spinel.[38] Their interest in spinel has been concerned with electronic applications; specifically, the substrate material for epitaxial silicon.

Crystal growth of low Al-rich spinel is achieved at RCA by the Verneuil flame-fusion technique using a Verneuil growth unit.[38] This unit consists of three major components: (1) the hopper, tapping and burner assembly, (2) the lowering mechanism, and (3) the gas system. The burner is a specially designed three-tube post mix type,

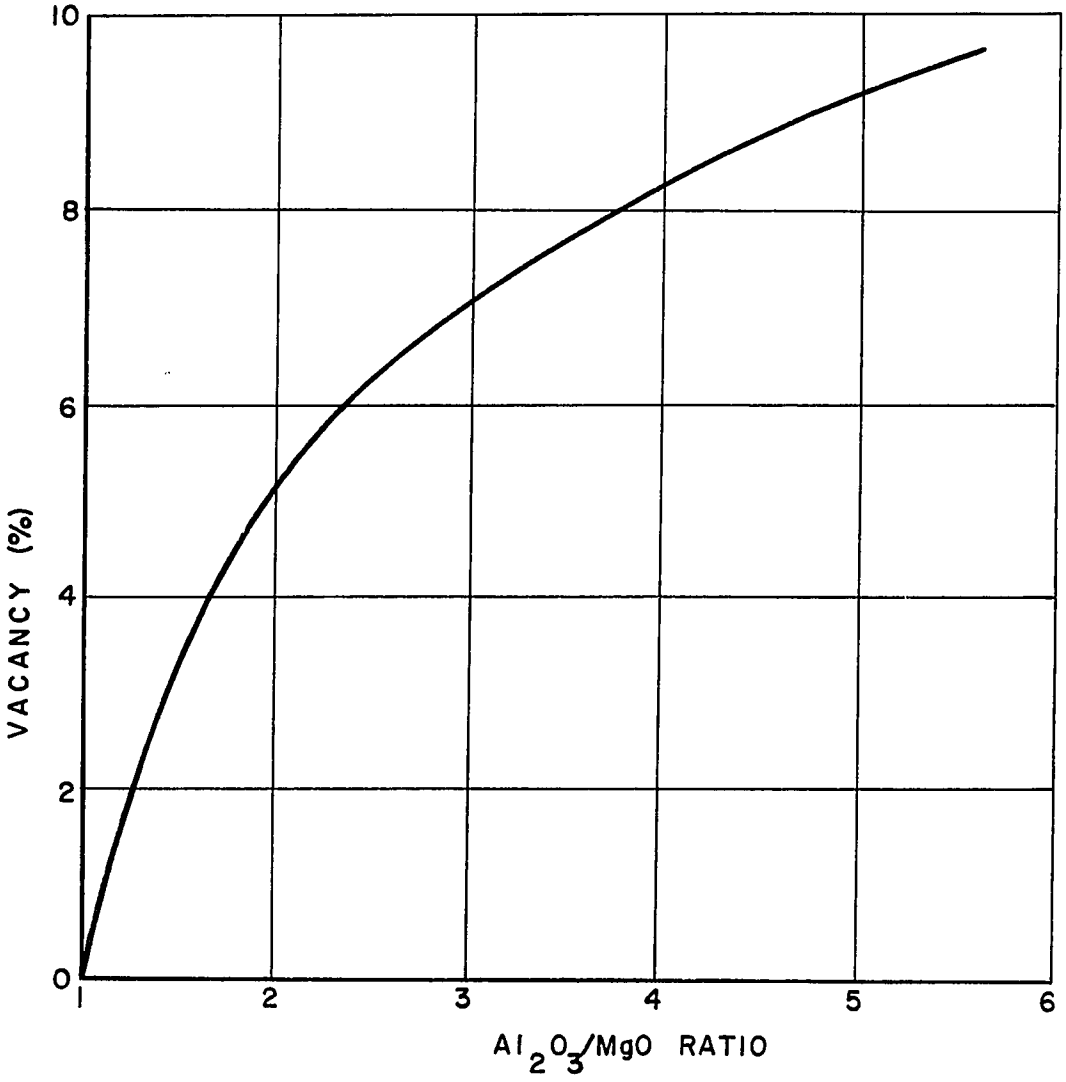

FIGURE 5. METAL ION VACANCY IN SPINEL.[6]

and provides a large controllable flame with minimum turbulence. Feed powder is prepared by calcining pre-determined mixtures of Al-rich ($Al_2(SO_4)_3 \cdot (NH_4)_2 \cdot 24H_2O$) and epsomite ($MgSO_4 \cdot 7H_2O$), both reagent grade from Baker Company. The calcining temperature is about 1100 ^oC.

Operational difficulties in growing the crystal have been overcome at RCA by utilizing a self-seeding powder cone technique. In starting crystal growth from a powder cone the seed emerging from the powder is the same material as that of the crystal to be grown. The growth temperature is about 2100 ^oC., the melting point of magnesium aluminate.

After growth of the crystal, the crystal is crushed and ground to very fine powder.

Stoichiometric spinel is grown by a flux technique[39] developed at the RCA Laboratories. Stoichiometric spinel grown by the Verneil flame-fusion method tends to crack during growth and/or mechanical processing.

Crystal growth is carried out in a crucible using a PbF_2 flux solvent and B_2O_3 as a liquid encapsulant. Vaporization of the flux at constant growth temperature (1250 ^oC) is used for the generation of supersaturation to promote the crystal growth. After the desired period of growth time, circulating air is used to cool the

crucible from the growth temperature to room temperature. A typical time for this method is 500 hours.

A growth mechanism has been postulated[40] to explain crystal growth by the flux technique. The first stage involves the dissolution of MgO and Al_2O_3 in PbF_2. The second stage is the precipitation of spinel from the supersaturated solution and growth by a diffusional transport reaction. Throughout both stages, the spinel crystals retain their stoichiometric composition, despite the losses of MgO and Al_2O_3 in the first stage to MgF_2 needles and α- Al_2O_3 platelets. An explanation of this may be that at the relatively low growth temperature, the stoichiometric composition is thermodynamically the only stable composition. (See phase diagram, Fig. 22, p. 120).

The single crystals were ground to a fine powder having a BET surface area of 35 m^2/gm. The surface area does not vary with composition.

E. Crystalline Perfection.

The crystal perfection of the spinel single crystals was characterized at RCA Laboratories by the Lang Method[41] of X-ray diffraction topography. This technique reveals any local variations in lattice perfection due to dislocations, stacking faults, impurity precipitates, growth striations, surface damage, and detects changes in lattice orientation due to strain. Very few of these defects were observed,

so that the general crystalline perfection of the single crystals must be characterized as very good. Imperfections caused by grinding the single crystal to fine powder were not examined.

Wang[42] illustrates the superior quality of the flux-grown spinel crystals by comparing them with flame-fusion and Czochralski melt-grown spinel crystals. A topograph of a commercial flame-fusion high Al-rich spinel ($MgO:3.3Al_2O_3$) from Wiede Carbidwerk, West Germany had a dislocation density so high that there was no resolution of individual dislocations. The dislocation density is probably higher than 10^5 lines/cm^2. A topograph of a commercial Czochralski "stoichiometric" spinel crystal from the Linde Company had individual dislocations that could be resolved; the average dislocation density of the melt-grown crystal observed was 3×10^3 lines/cm^2. A topograph of two flux-grown stoichiometric spinel crystals from RCA had average dislocations of less than 50 lines/cm^2. Diffuse straight lines appeared in the topograph and are due to surface scratches. A third RCA crystal examined had a dislocation density of 200 lines/cm^2. Stacking faults were observed in wafers from flux-grown crystals.

Crystals grown by flame-fusion show remarkable perfection in that no twins and/or stacking faults are observed from electron diffration patterns. Evidence was present that these crystals are strained.

Impurities typically scattered at random throughout the non-stoichiometric crystals are (in ppm by weight): Cu (0.3-3), Fe (10-100), Ga (6-60), and Si (100-1000). The high silica content is caused by contamination from the silica vessel used to prepare the feed powder. The impurity content of stoichiometric crystals is (in ppm by weight): Ag (3-30), Fe (10-100), Ga (3-30),Si (0.3-3) and Pb (30-300). The Pb content has been reduced to the given value by thermal treatment at 1200 ^{o}C and 10^{-6} torr for one hour.

F. Mathematical Modeling of Kinetic Reactions.

There have been numerous approaches to mathematical modeling of kinetic mechanisms. Notable among modeling techniques was the early work of Hougen and Watson based on Langmuir-Hinshelwood activated adsorption surface reaction mechanisms. These authors postulated "hyperbolic" equations of the form

$$r = \frac{(\text{kinetic term})(\text{potential term})}{(\text{adsorption term})^{n}}$$

These equations involved both kinetic rate constants and adsorption constants. The equations were linearized and parameter estimates were carried out by linear least squares analysis.(44)

Another engineering approach to the mathematical modeling of kinetic rate data is the power law equations used by Levenspiel and Smith.(45) This approach does not concern itself with the mechanism of the reaction but rather attempts a direct correlation of experimental data with equations of the form

$$-r = kC^n$$

where r is the rate of reaction, C is the concentration, k is the kinetic rate constant, and n is the order of the reaction. Experimental concentration or conversion versus time data may be fitted to the integrated form of this equation.

A third approach to mathematical modeling is possible if experimental conditions can be arranged such that the adsorption rate constants as used by Hougen and Watson can be ignored. It is then possible to write differential equations directly from the postulated surface controlling mechanism. This method is favored in the journals specifically concerned with catalysis.[46]

A problem (now considered classic) investigated by Hougen and Watson[47] was the hydrogenation of iso-octene:

$$C_8H_{16}(g) + H_2(g) \rightleftharpoons C_8H_{18}(g)$$

Hougen and Watson postulated eighteen possible mechanisms. Model discrimination techniques (utilizing linear least squares) available at the time eliminated all but one mechanism. Sixteen equations were rejected because some coefficients had negative values according to the least squares calculations, where they should have been positive to have physical justification, and some coefficients had finite values when they should not appear in the equation at all. The seventeenth equation was rejected because of statistically poorer fit to the data.

The method of arriving at the decision to reject all equations with poorer fit to the data and accept the best equation has been criticized.[48] When one equation may represent the data to the same degree of closeness as another, there is no reason to reject the former unless all possibilities are eliminated. Merely because some coefficient is not the desired value, or has an opposite sign, should not eliminate this possibility.

Blakemore and Hoerl[49] analyzed the hydrogenation of iso-octene data originally analyzed by Hougen and Watson via linear least squares. These authors showed by non-linear least squares analysis that it is impossible to select any one model as being the best model of the entire set.

Hougen and Watson rejected many of their models for possessing negative adsorption or rate constants. These should not have been rejected on this basis, for through a non-linear least squares analysis of the same data, many of these constants are found to be positive.[50] The non-linear analysis essentially provides a different assumption about the proper weighting of the data, felt to be more justifiable from an experimental point of view, namely, that the errors in the rate measurements are approximately constant.

The linear least squares analysis as used by Hougen

and Watson does not minimize the sum of squares of residuals of the reaction rates but rather that of a combination of the rate and the independent variables, the error distribution for which is not necessarily as obvious.

A recently developed method to analyze data is called non-linear least squares data analysis. This method utilizes statistical information, such as confidence limits, standard error, and the covariance matrix to discriminate between possible mechanisms of the catalytic reaction.

Non-linear parameters are analyzed in statistical methodology by non-linear least squares regression analysis. The basic idea of non-linear least squares is simple. It consists of finding those values of the parameters $\underline{K}$ in the model $\eta = f(X,K)$ which will make the calculated values agree as closely as possible in a least squares sense with the actually observed values; that is, the minimum of the sum of squares function must be found. This involves an iterative search procedure using a digital computer. The estimation process is much more laborious and time-consuming than that of linear least squares.

Two groups have done considerable work on non-linear

least squares parameter estimates of kinetic constants: one group at the University of Wisconsin consists of J.R. Kittrell, W.G. Hunter and C.C. Watson;[52] the second group at Princeton University consists of L. Lapidus and T.I. Peterson.[53] The pioneer mathematician who has been instrumental in optimization techniques and statistical analysis as used in non-linear least squares regression analysis has been G.E.P. Box.[54] Excellent reviews concerning estimation of parameters by non-linear least squares analysis are available in the papers by Lapidus,[55] Shah,[56] and Kittrell.[57]

There are at present four computer programs available for non-linear least squares analysis.[58]

1. The Lapidus-Peterson program.[59] This program is suitable for the IBM 7090/94 computers. It features a kinetics language for input of the kinetic reaction model and experimental data, a differential equation solver for numerical integration of the rate equations and a non-linear estimation algorithm for obtaining least squares estimates of the parameters via the Gauss Method.[60]

2. The Eisenpress-Greenstadt non-linear maximum likelihood program.[61] This program is suitable for the IBM 7090/94 computers. The program is applicable to kinetics problems only where differential rate measurements are available or when analytic solutions to the rate

equations are available.

3. The Bard non-linear parameter estimation program.[62] This program is written in Fortran IV. The program solves non-linear least squares, weighted least squares, maximum likelihood, and Bayesian estimation problems. It uses the generalized Gauss-Newton method,[63] or optionally, the Davidson-Fletcher-Powell method.[64]

4. The Marquardt program.[65] This program is written in Fortran IV. It uses Marquardt's compromise method.[66] The user may supply analytic derivatives, or, optionally, the program will calculate the derivatives numerically. The user must also supply the model $\eta = f(\underline{X},\underline{K})$ to be fitted and the data, together with initial guesses for the parameters $\underline{K}$. The program output lists the observed value of the dependent variable, y, the computed value of the dependent variable, $\underline{y}$, an estimate of variance based on the residuals, an approximate confidence interval for each of the parameters and other statistical information.

CHAPTER III

REACTION MECHANISMS FOR THE COCM

A. Rate Steps in the Oxidation Process.

For any heterogeneous catalytic reaction, and for the particular reaction under consideration, the oxidation of carbon monoxide, it is generally agreed (67) that the following sequence of rate steps is possible:

1. Reactant molecules of carbon monoxide and/or oxygen must diffuse from the bulk gas phase to the exterior surface of the catalyst. The resistance to diffusion occurs at the gas boundary layer near the solid surface.

2. The reactant molecules, having reached the catalyst surface, must diffuse through the catalyst pores. In addition to ordinary molecular diffusion, Knudsen diffusion may occur. Knudsen diffusion occurs when the pore diameter is smaller than the mean free path of the gas molecules.

3. A reactant molecule is chemisorbed through the formation of an activated complex with an active site. Alternatively, two different reactant molecules may be chemisorbed to form dual active sites.

There are three possibilities for the type of bond of a chemisorbed particle with a solid surface: (1) "weak" bond, (2) "strong" acceptor bond, and (3) "strong" donor

bond. Garner and Hauffe[68] introduced the idea of acceptor and donor reactions. With a "weak" bond, an electron of the chemisorbed particle is drawn close to a cation of the lattice or an electron of the anion of the lattice is drawn close to the chemisorbed particle. The latter remains electrically neutral. With a "strong" acceptor bond, an electron of the particle adsorbed on the cation interacts with a free electron of the semiconductor, thus bringing about a chemical bond with the lattice. With a "strong" donor bond, an atom or molecule is adsorbed on an atom of the lattice and enters into an interaction with a free hole (i.e., the transfer of an electron proceeds from the adsorbed particle to the catalyst) of the semiconductor.

4. The adsorbed reactant molecule reacts with reactant in the gas phase to form chemically adsorbed products. Alternatively, two adsorbed molecules on dual sites react to form chemically adsorbed products. The products formed need not necessarily be adsorbed, but may be released directly.

5. The product molecules (carbon dioxide) are activated and desorb from the active site.

6. The product molecules diffuse through the catalyst pores to the bulk gas phase.

7. The product molecules diffuse through the gas film boundary on the catalyst surface to the gas bulk phase.

All of these rate steps could be contributing to the

rate of a reaction-process. It is often found, however, that one step is much slower than any of the others, and hence controls the rate process. With only one rate step involved, the analysis of the reaction process is greatly simplified.

In this work, it was desired to study rate step 4, the surface-reaction controlling step. It would be desirable to eliminate the other five steps to simplify analysis. This could be arranged by designing experiments in the proper fashion; this will be considered in Chapter IV. For now, it is agreed to consider rate steps 1,2, 3, 5 and 6 to be fast, and rate step 4, the surface-reaction step, is controlling the oxidation process.

B. Mechanism of the Surface Controlled Reaction.

Having agreed in the last section that the surface reaction be the slow step in the oxidation reaction, the next strategic move should be to determine the mechanism of the surface reaction.

It is possible that more than one reaction is occurring on the catalyst surface. It is desirable to classify the magnitude of reaction between one mechanism and another. The magnitude of reaction may be classified as primary or secondary.

1. Primary Reaction. This shall refer to the main reaction occurring on the catalyst surface.

Since magnesium aluminate is an insulator, the number

of free electrons or holes is negligible. Hence "strong" chemisorption is not probable; the probability is quite high that either carbon monoxide or oxygen is "weakly" chemisorbed. The type of chemisorption is best distinguished by measuring the heats of adsorption (higher for "strong" chemisorption); this work was not undertaken in experimentation.

Considering first the case where carbon monoxide is "weakly" chemisorbed, the reaction can be written

$$(^{*}CO\text{-}Si_2) + O_2(g) + Si_1 \longrightarrow {}^{*}CO_2 + (O\text{-}Si_1) + Si_2 \qquad (1)$$

where Si_1 denotes active site number one, etc.

Compare Equation (1) with the case where oxygen is "weakly" chemisorbed,

$$^{*}CO(g) + (O\text{-}Si_1) \longrightarrow {}^{*}CO_2(g) + Si_1 \qquad (2)$$

Experimental evidence in favor of Eqn. (2) was provided by pretreating catalyst samples with non-radioactive and radioactive gas mixtures. Comparision of the rate of reaction on the different pretreated catalysts showed that there was negligible difference in the rate of reaction. This indicated that CO adsorption was negligibly small.

Balandin[69] considered the reaction of Eqn. (1) in studies of CO oxidation on NiO catalysts. He found that no reaction occurs on the NiO surface previously saturated with chemisorbed carbon monoxide if the oxygen pressure is only 10 mm. Hg. Balandin concluded that the reaction of Eqn. (1) is not possible. At higher pressures of oxygen, as

conductivity measurements show, adsorption of O_2 takes place and promotes the catalytic oxidation of CO. This author also concluded that an oxygenated surface promotes CO oxidation, while a surface of NiO covered with CO precluded oxidation. All intermediate stages of coverage are possible but increasing CO coverage contributes to the increased activation energy of the catalytic reaction.

The reaction of Eqn. (2) is consistent with the results of Wagner and Hauffe.[70] These authors, on the basis of semiconductivity data, concluded that the controlling step for the CO oxidation on NiO at 700 °C is determined by the rate of CO interaction with the NiO surface. Parravano[71] also found the reaction of Eqn. (2) to be rate controlling on NiO in the temperature range of 160 to 222 °C.; however, the rate controlling step was dependent upon the concentration of excess oxygen in the solid phase.

It is concluded that the primary reaction is represented by Eqn. (2); the radioactive carbon monoxide reacts with a "weakly" chemisorbed oxygen molecule to form radioactive carbon monoxide and a vacant active site.

2. Secondary Reactions. In addition to the primary reaction, there may be reactions occurring on a scale of magnitude much less than the primary reaction. These reactions must be considered because they may exert an influence on the correlation of the primary reaction with experimental data.

Three secondary reacions may be envisioned:

a. The reaction of Equation (2) may be more or less reversible:

$$^{*}CO_2 + (Si_1) \longrightarrow {}^{*}CO(g) + (O\text{-}Si_1) \qquad (3)$$

The following values pertain to the reaction

$$CO(g) + \tfrac{1}{2}O_2 \rightleftharpoons CO_2 : {}^{(72)} \qquad (4)$$

T (°C)	K_p	ΔF (cal)
500	1.82×10^{14}	-21850
600	3.55×10^{12}	-21700

where the equilibrium constant, K_p, is defined as

$$K_p = P_{co_2}/(P_{co}\sqrt{(P_{o_2})})$$

The negative free energy (ΔF) values signify that the reaction is spontaneous in the forward direction. The large values for K_p signify that the reaction is essentially irreversible.

Experimental data at long periods from the start of a reaction indicate that the oxidation reaction goes to completion.

b. A "weakly" adsorbed radioactive carbon monoxide molecule reacts with oxygen which is "weakly" adsorbed on an adjacent site to produce radioactive carbon dioxide and two vacant sites,

$$(^{*}CO\text{-}Si_2) + (O\text{-}Si_1) \longrightarrow {}^{*}CO_2(g) + (Si_1) + (Si_2) \qquad (5)$$

El Shobaky, Gravalle and Teichner[73] found Equation (5) to be rate controlling in their study of carbon monoxide oxidation on a blend of NiO denoted as NiO(250).

c. Radioactive carbon monoxide in the gas phase reacts with "weakly" chemisorbed carbon monoxide to produce radioactive carbon dioxide and a site poisoned with carbon:

$$^{*}CO(g) + (CO\text{-}Si_2) \longrightarrow (C\text{-}Si_2) + {}^{*}CO_2(g) \qquad (6)$$

Taylor and Burwell[74] accumulated considerable evidence that the formation of CO_2 resulted from the disproportionation of the type denoted by Equation (6). On continued treatment with carbon monoxide, their adsorbent (ZnO) became gray-brown. The color change became obvious only after some hours. The original white color of the oxide was restored by treatment with hydrogen by a process which suggested the conversion of carbon to methane. The carbon was clearly not bulk graphite but probably represented small atomic clusters which may almost be considered to be adsorbed carbon.

C. Derivation of Mathematical Models.

Mathematical models can be derived from the mechanisms postulated in the previous section.

1. Model One. This model is based on Primary Reaction One:

$$^{*}CO(g) + (O\text{-}Si_1) \xrightarrow{k_1^{*}} {}^{*}CO_2(g) + (Si_1) \qquad (2)$$

The corresponding fast reaction for the regeneration of adsorbed oxygen is

$$O_2(g) + 2(Si_1) \rightleftharpoons 2(O\text{-}Si_1) \qquad (7)$$

The rate of disappearance of $^{*}CO$ may be written:

$$-dP_{*co}/mdt = k_1^{*}(O\text{-}Si_1)\, P_{*co}$$
$$= k_1' P_{*co} \qquad (8)$$

where k_1' results from the assumption that the concentration of oxygen sites is constant; m is the mass of catalyst, in grams. The units of k_1' are $(\text{hr.(gm. of catalyst)})^{-1}$.

Defining $$f_{*co} = P_{*co}/P_{*c} \tag{9}$$

where $$P_{*c} = P_{*co} + P_{*co_2} \tag{10}$$

The following integral may be written:

$$\int_1^{f_{*co}} df_{*co}/f_{*co} = -mk_1' \int_0^t dt \tag{11}$$

The resulting solution is

$$f_{*co} = \exp(-k_1 t) \tag{12}$$

where $k_1 = mk_1'$ (hr.(m gm. of catalyst))

2. Model Two. This model is based on Primary Reaction 1 in parallel with Secondary Reaction 1:

$$^*CO(g) + (O\text{-}Si_1) \xrightarrow{k_1^*} {}^*CO_2(g) + (Si_1) \tag{2}$$

$$^*CO_2 + (Si_1) \xrightarrow{k_2^*} {}^*CO(g) + (O\text{-}Si_1) \tag{3}$$

The adsorbed oxygen is also regenerated by the fast reaction given by Equation (7).

The rate of disappearance of $^*CO$ may be written:

$$-dP_{*co}/mdt = k_1^*(O\text{-}Si_1)P_{*co} - k_2^*(Si_1)P_{*co_2}$$

$$= k_1'P_{*co} - k_2'P_{*co_2} \tag{13}$$

where k_1' and k_2' result from the assumption that the concentration of adsorbed oxygen sites, and the concentration of empty oxygen sites, respectively, is constant.

The total pressure of radioactive carbon species is given by Eqn. (10). Define f_{*co} as in Eqn. (9). Then,

$$P_{*co_2}/P_{*_c} = 1 - f_{*co} \qquad (14)$$

The differential equation may be written in terms of f_{*co},

$$-df_{*co}/mdt = k_1' f_{*co} - k_2'(1 - f_{*co}) \qquad (15)$$

Rearranging the last equation and taking integrals,

$$\int_1^{f_{*co}} df_{*co}/(m((k_1' + k_2')f_{*co} - k_2')) = -\int_0^t dt \qquad (16)$$

Integrating, the solution is

$$f_{*co} = (k_1/(k_1 + k_2)(\exp(-(k_1 + k_2)t) + k_2/k_1)) \qquad (17)$$

where $k_1 = mk_1'$

$k_2 = mk_2'$ $\quad (\text{hr.}(\text{m gm. catalyst}))^{-1}$

3. Model 3. This model is based on Primary Reaction 1 in parallel with Secondary Reaction 2:

$$^*CO(g) + (O\text{-}Si_1) \xrightarrow{k_1^*} {}^*CO_2 + (Si_1) \qquad (1)$$

$$(^*CO\text{-}Si_2) + (O\text{-}Si_1) \xrightarrow{k_2^*} {}^*CO_2(g) + (Si_1) + (Si_2) \qquad (5)$$

The adsorbed oxygen and carbon monoxixe sites are regenerated by the fast reactions,

$$O_2(g) + 2(Si_1) \longrightarrow 2(O\text{-}Si_1) \qquad (18)$$

$$CO(g) + (Si_2) \longrightarrow (CO\text{-}Si_2) \qquad (19)$$

$$^*CO(g) + (Si_2) \longrightarrow (^*CO\text{-}Si_2) \qquad (20)$$

The rate of reaction is the same for the reactions of Eqns. (19) and (20); the distinction is made between $^*CO$ and CO because the concentration of CO is much greater than that of $^*CO$, and hence the mass amount of reaction is greater in Equation (19).

Differential equations may be written for the disappearance of carbon monoxide:

$$-dP_{*co}/mdt = k_1^*(O\text{-}Si_1\ P_{*co} + k_2^*(^*CO\text{-}Si_2)(O\text{-}Si_1)$$

$$= k_1'P_{*co} + k_2' \qquad (21)$$

The constants k_1' and k_2' result from the assumption that the concentration of adsorbed oxygen sites, and the concentration of adsorbed carbon monoxide sites, respectively, is constant.

Defining f_{*co} as in Equation (9), Equation (21) may be written as

$$-df_{*co}/dt = k_1 f_{*co} + k_2 \qquad (22)$$

where

$$k_1 = k_1'm \qquad (\text{hr.}(\text{m gm. catalyst}))^{-1}$$

$$k_2 = mk_2'/P_{*c} \qquad \frac{\text{atm.}}{(\text{hr.}(\text{m gm. catalyst})}$$

The differental equation, Equation (22), may be integrated:

$$\int_1^{f_{*co}} df_{*co}/(k_1 f_{*co} + k_2) = -\int_0^t dt \qquad (23)$$

The solution to this equation is given by

$$f_{*co} = ((k_1+k_2)\exp(-k_1 t) - k_2)/k_1 \qquad (24)$$

4. Model 4. This model is based on Primary Reaction 1 in parallel with Secondary Reaction 3:

$$^{*}CO(g) + (O\text{-}Si_1) \xrightarrow{k_1'} {}^{*}CO_2(g) + (Si_1) \qquad (2)$$

$$^{*}CO(g) + (CO\text{-}Si_2) \xrightarrow{k_2'} (C\text{-}Si_2) + {}^{*}CO_2(g) \qquad (6)$$

The adsorbed oxygen and carbon monoxide sites are regenerated by the fast reactions given by Equations 18, 19 and 20.

The rate of disappearance of $^{*}CO$ may be written,

$$-dP_{*co}/mdt = k_1'(O\text{-}Si_1)P_{*co} + k_2'(Co\text{-}Si_2)P_{*co}$$

$$= k_1 P_{*co} + k_2 P_{*co}$$

$$= (k_1 + k_2)P_{*co}$$

$$= k\, P_{*co} \qquad (25)$$

The constants k_1' and k_2' result from the assumption that the concentration of adsorbed oxygen, and the concentration of adsorbed carbon monoxide, respectively, are constant. This differential equation is identical to the differential equation of Model One. Hence the solution will be identical and Models One and Four will be indistinguishable from one another without experimental evidence. There was no experimental evidence of a darkening of catalyst as would be caused by adsorbed carbon sites.

The "weak" adsorption of oxygen in these models is presumed to be the mobile form of oxygen adsorption observed by Garner, Gray and Stone in their studies of oxygen adsorption on Cu_2O films.[94]

CHAPTER IV

EXPERIMENTAL

A diagram of the apparatus used for the catalytic oxidation of carbon monoxide (COCM) is shown in Figures 6 and 7, in which all the major components are identified. The apparatus was tested and shown to maintain a vacuum of 10^{-5} torr over several days in all sections not exposed to mercury.

Coleman grade carbon dioxide, research grade carbon monoxide, and research grade oxygen (by Matheson Company, Inc.) were introduced into storage spheres after it was confirmed that the connections from the gas cylinder to the sphere were vacuum tight. The connections were first degassed to remove contaminants and then purged several times with gas and evacuated to further reduce the presence of contaminants. A gas mixture, the composition of which was achieved by pressure measurement of the constituents carbon monoxide, carbon dioxide, and oxygen, was stored in the fourth storage sphere. The composition of the gas mixture was 50% CO_2, 25% CO, and 25% O_2. (mole %)

Radioactive carbon monoxide of 1.0 millicurie radiation was supplied in a sealed glass tube ampoule by New England Nuclear Corporation. A small iron rod was placed

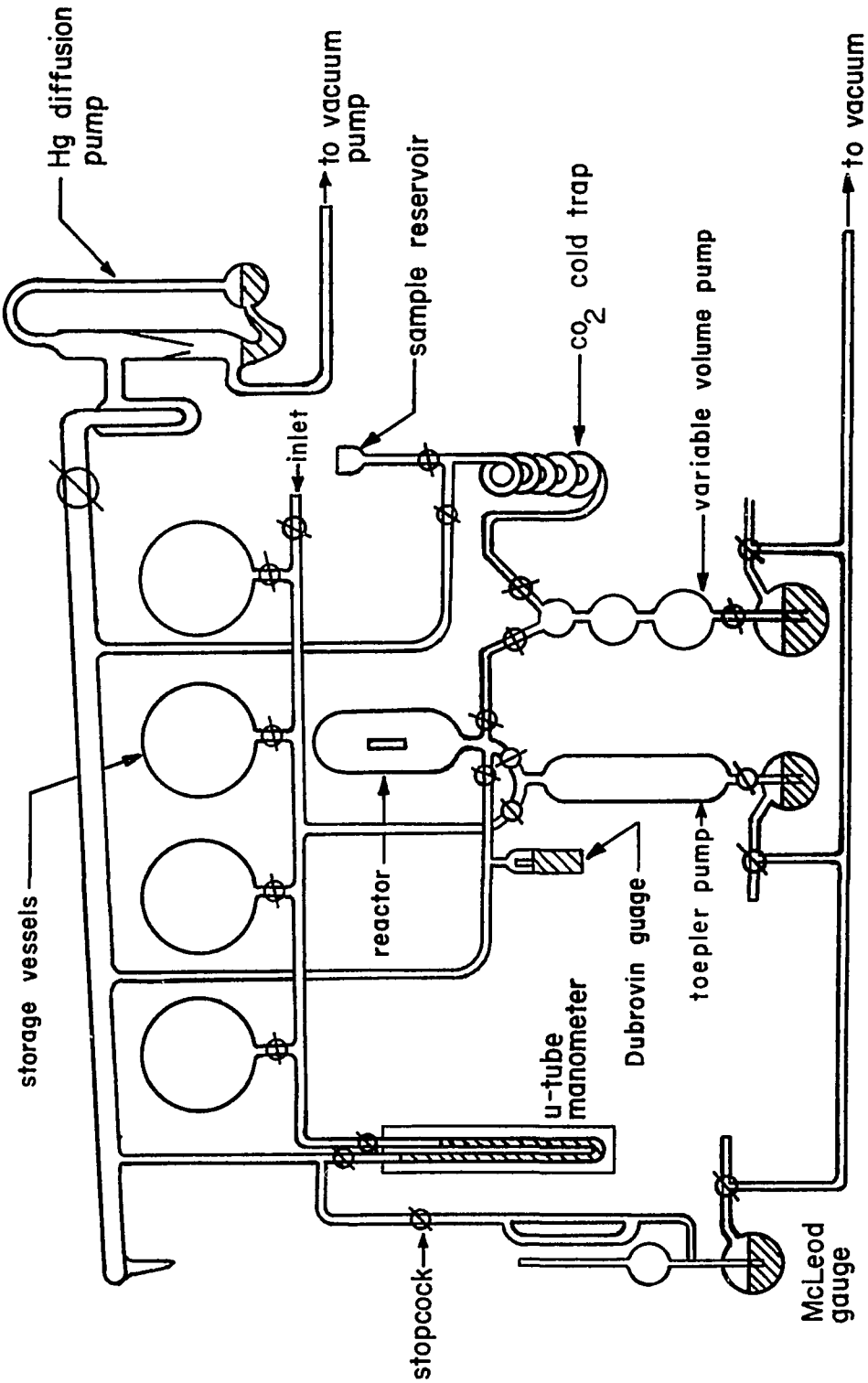

Figure 6. Apparatus for the catalytic oxidation of carbon monoxide.

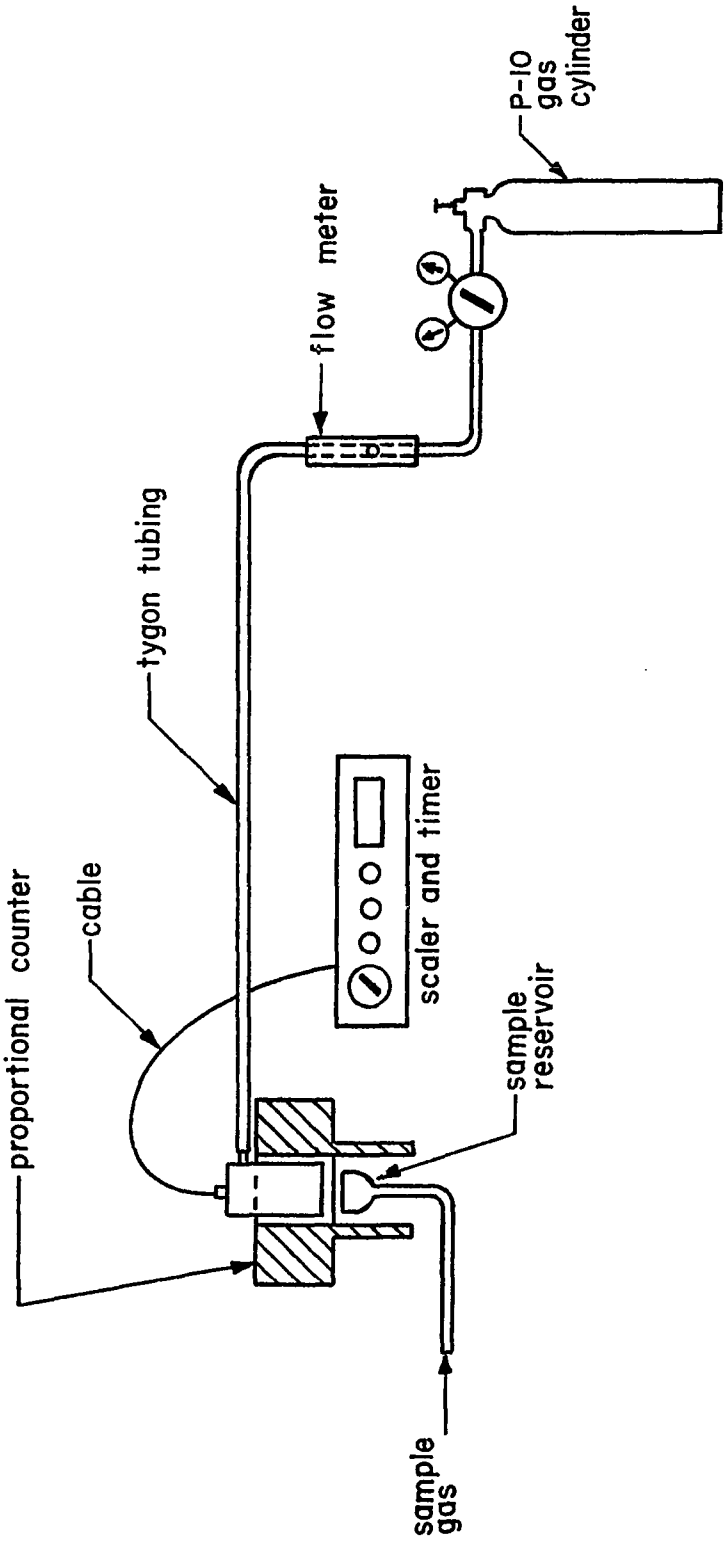

Figure 7. Proportional counter and accessories.

in the entrance to the sealed glass tube. The glass tube was fused to the apparatus at the inlet shown in Figure 6. After evacuating the system to 1 x 10^{-5} torr, a magnet was used outside the tubing to move the iron rod which broke the tip of the sealed glass tube. This operation released the carbon monoxide gas into the Toepler pump. The radioactive carbon monoxide ($^{*}CO$) gas was mixed with the gas mixture in the Toepler pump and then stored in a storage sphere. The small amount of $^{*}CO$ was assumed to mix homogeneously with the larger amount of CO present. Four hours were allowed for mixing to insure adequate diffusion of $^{*}CO$ in CO.

The reactor, constructed of quartz glass, measured 3 inches in diameter by 18 inches long, and had a volume of 1844 ml.It was attached to the apparatus with a detachable connecting tube. The reactor was placed in a three zone furnace manufactured by Lindberg (54000 Series). The three zones were controlled with a 59000 Series Control console by Lindbergh. In order to establish uniform temperature throughout the reactor, the furnace had to be balanced by adjusting the controller. Three thermocouples were placed on the outside of the reactor: at the ends and in the center of the reactor. The furnace was adjusted so that the three thermocouples were within 1 $^{o}C.$ of each other. Whenever the reactor temperature was varied, at least eight hours were allowed to ellapse for the reactor

to reach uniform temperature.

A 0.3000 gram sample of magnesium aluminate catalyst was precisely weighed, loaded into a ceramic boat and placed in the center of the reactor. No attempt was made to condition the sample to constant relative humidity before placing it in the reactor. The catalyst was outgassed at 600 ^{o}C. for twenty-four hours under a pressure of 1 x 10^{-5} torr. This operation removed adsorbed contaminants and also established a uniform surface area. After outgassing, the temperature was lowered to the temperature desired for an experiment. A gas mixture of concentration equal to the stored gas mixture, but without *CO, was stored in another sphere for use in pretreating the catalyst surface. The catalyst was pretreated statically for 12 hours to allow the surface to equilibrate. The reactor was then evacuated at 1 x 10^{-5} torr for three minutes, and the experiment was started by introducing the radioactive gas mixture into the reactor. A gas sample was withdrawn to the sampling Toepler pump for analysis after ellapsed intervals of time. The time interval depended on the rate of the reaction.

A flow counter (Model No. FD-1 Gas Flow Counter by Tracerlab, Inc.) was used for the measurement of soft beta radiation from *CO in the gas mixture. The count gas used in the flow counter was P-10 gas (90% argon, 10% methane). A 132 MA Manual Scaler, also by Tracerlab, was

employed to amplify and register the radiation (see Figure 7).

The gas sample was pumped to a reservoir with a mica window below the flow counter to count the total $^{*}CO_2$ and $^{*}CO$ in the gas. The sample reservoir (see Figure 7), with a glass flange on the top end, was made of a piece of 30 mm. OD glass tubing about 38 mm. long with a flat glass bottom. The top end was sealed by a mica window with a density of 6.0 mg./cm^2. The sealant was an epoxy cement supplied by the Borden Company. The sample gas was pumped back and forth three times through the CO_2 trap at liquid nitrogen temperature to condense the CO_2 and $^{*}CO_2$ from the gas mixture. Then the $^{*}CO$ was counted in the reservoir. The total count of $^{*}CO_2$ and $^{*}CO$ was corrected from the background count automatically by the manual scaler. The $^{*}CO$ count was corrected from both the background count and the residue $^{*}CO$ count which was obtained before the experiment. The residue count is necessary because of the partial solubility of $^{*}CO$ in the liquified CO_2. A calibration curve (see Figure 8) was determined experimentally to correct for the $^{*}CO$ lost in liquified CO_2. Since the curve is linear, an equation was developed from linear least squares so that this correction could be calculated accurately rather than

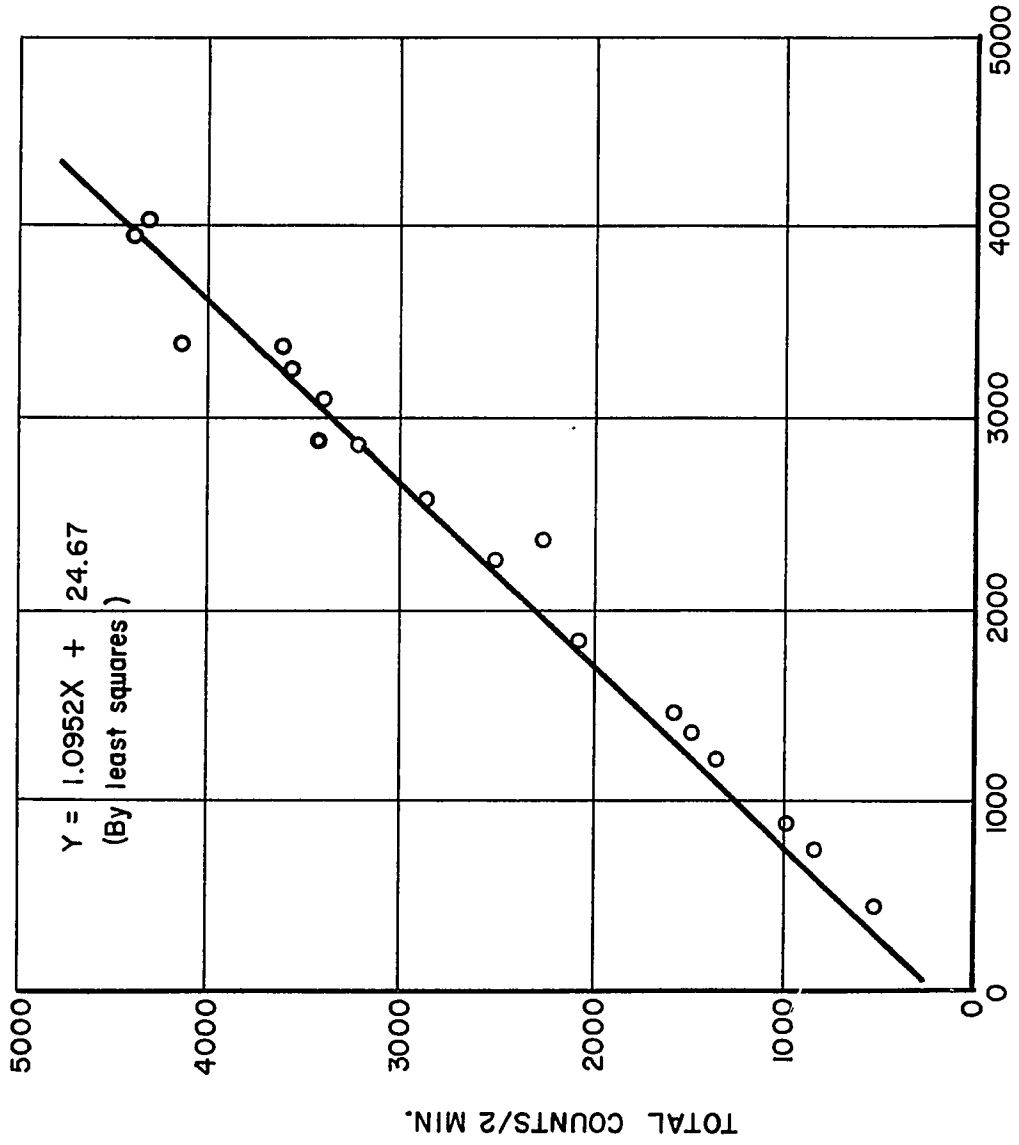

Figure 8. Correction for separation of $^{*}CO$ from $^{*}CO_2$ by freezing. (Correction allows for the solubility of $^{*}CO$ in $^{*}CO_2$.

obtained haphazardly by graphical means.

The fraction of $^{*}CO$ in the gas phase is calculated from the relationship

$$f_{*_{CO}} = Z/X \qquad (26)$$

where Z = $^{*}CO$ count after reaction and freeze separation.

X = Corrected $^{*}CO$ count, after reaction, before freeze separation.

The value of X in this equation is obtained from the calibration equation,

$$Y = 1.0952\ X + 24.67 \qquad (27)$$

Approximately 1.7% of gas in the reactor was removed for each analysis. This amount could not be transferred back into the reactor.

The initial amount of gas mixture was the same for each experiment. The initial pressure for each experiment was 9.0 torr. The temperature range for the reaction varied from 500 ^{o}C. to 600 ^{o}C.

The effect of pore diffusion was kept at a minimum by using finely powdered catalyst. Calculations are presented in Appendix IV showing that pore diffusion and molecular diffusion are negligible; the oxidation reaction is shown to be controlled by the surface reaction.

CHAPTER V

RESULTS AND DISCUSSION

A. Experimental Results.

The strategy employed in determining the best experimental conditions under which the oxidation reaction should be studied is illustrated by use of a logic diagram as shown in Figure 9.

Since quartz may act as a catalyst for the oxidation of carbon monoxide, it was necessary to determine if the oxidation reaction was being influenced significantly by the quartz reactor.(75) A study was made without a catalyst sample in the quartz reactor. It was found that a 12 hour pretreatment of the reactor with reactant gas has a critical effect on the oxidation reaction. First, reaction was attempted with no pretreatment. There was no significant reaction at or below 500 °C. As the temparature was raised above 500 °C, the reaction commenced around 575 °C. At 600 °C the reaction went to completion in one half hour. Next the reactor was pretreated with reactant gas for 12 hours. No significant reaction was observed throughout the temperature range from 500 °C to 600 °C. It was concluded at this point that the pretreatment of the quartz reactor was critical if a catalyst sample was to be examined in this temperature range.

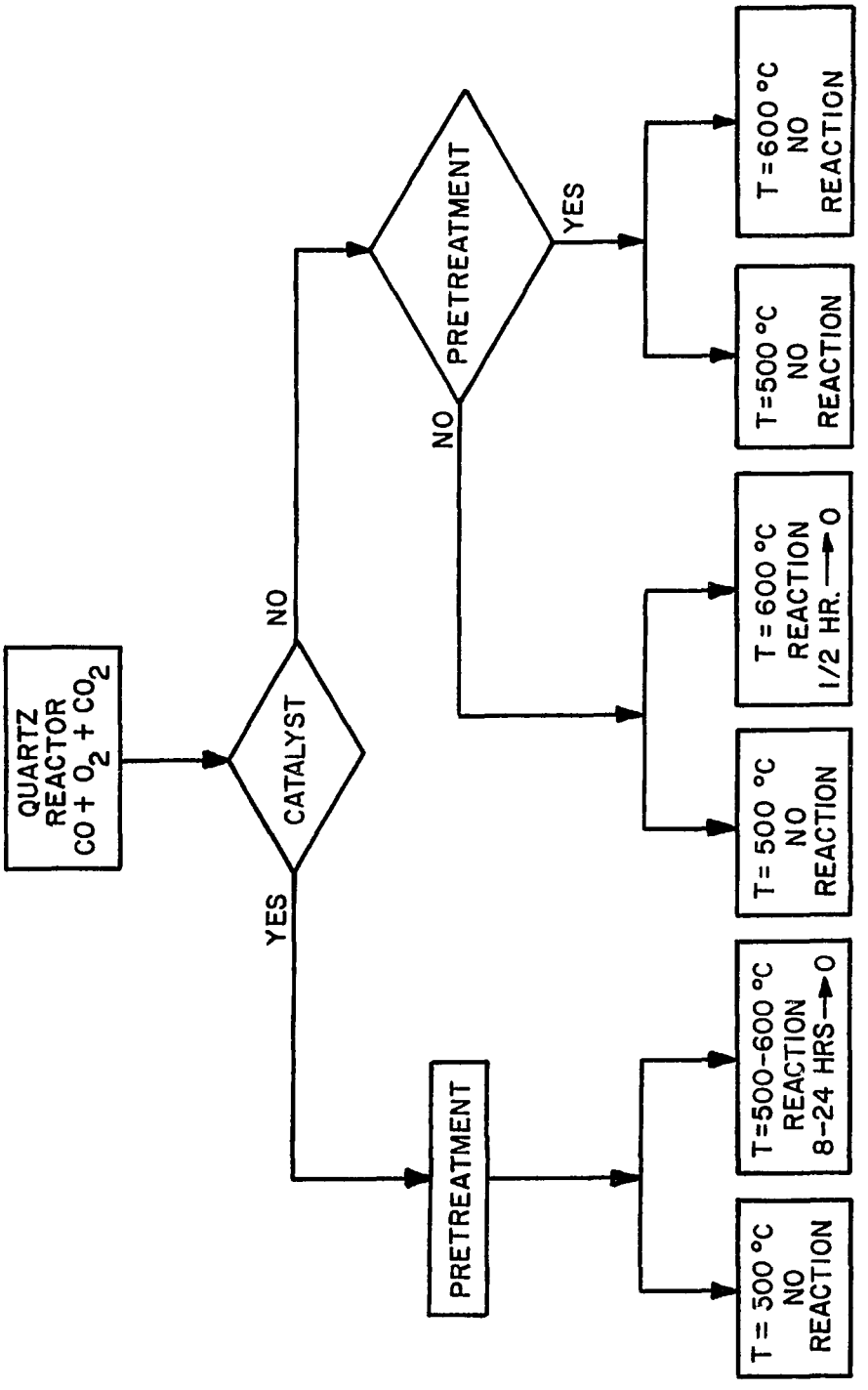

FIGURE 9. LOGIC DIAGRAM OF EXPERIMENTAL STRATEGY.

Having determined that the catalytic effect of the quartz could be ignored if the quartz was pretreated with reactant gas, it was now safe to assume that the entire catalytic effect of reaction would be due to the catalyst sample. With this in mind, catalysis studies were initiated using magnesium aluminate as the catalyst.

The first study with the catalyst sample was to determine the effect of pretreatment on the catalyst. The pretreatment with reactant gas was carried out by equilibrating the sample statically for 12 hours. The oxidation reaction was then observed over the temperature range from 500 °C. to 600 °C. Below 500 °C. the reaction was not initiated. At 500 °C. the reaction proceeded very slowly to completion in 6-8 hours. It was decided to study the effect of composition changes of magnesium aluminate in the temperature range 500-600 °C.

A study was made to determine the reproducibility of data. Repeat runs were made on the same catalyst sample to determine if a steady state condition existed on the catalyst surface. Steady state conditions are confirmed if the same results are obtained for each run. It was found that the catalyst reached steady state conditions quickly after one or two treatments with reactant gas.

The results for five catalyst samples, each of different composition and run at four different

temperatures, are tabulated in Appendix I, and presented in graphical form in Figures 10-14.

There was no color change in the catalysts after reaction as would be expected with Model 4 in which there is carbon formation.

B. Evaluation of Mathematical Models.

Marquardt's program[65] was used to apply non-linear least squares regression analysis for parameter analysis to the experimental data and the mathematical models because of its availibility.

The results from non-linear least squares regression analysis are tabulated in Appendix II. In these tables, the parameter estimates for each model are presented; also tabulated with each parameter is its confidence interval (95% level), its standard error (S.E.), and the optimized sum of squares of residuals, PHI.

Analytic derivatives are provided by Marquardt's program in the form

$$P^{(n \times k)} = (\partial f_i / \partial b_i) \tag{28}$$

The matrix

$$A = P^T P \tag{29}$$

is called the coefficient matrix of the normal equations. The C-matrix is then computed,

$$C = A^{-1} \tag{30}$$

The C-matrix, when multiplied by the sample variance, s_e^2, estimates the variance-covariance matrix of the parameter

estimates, b_j. If this matrix is diagonal, then the parameters are uncorrelated, the axes of the confidence ellipsoid are parallel to the coordinate axes. In the more usual case the C-matrix is not diagonal. The extent of the correlations among the parameter estimates is displayed by the elements of the parameter correlation matrix, R:

$$R = c_{jj'}/(\sqrt{c_{jj}}\sqrt{c_{j'j'}}) \qquad (31)$$

Whenever non-zero correlations exist, one-parameter confidence limits will underestimate the true interval within which a parameter B_j may lie and still remain within the confidence interval.

The parameter correlation matrices for these models were highly correlated; in general the values for the parameter correlation matrix are

$$\begin{bmatrix} 1.0000 & .9500 \\ .9500 & 1.0000 \end{bmatrix}$$

The confidence intervals of such models are regarded as accurate. A rule of thumb for 95% confidence intervals is that the confidence length should be approximately four times the standard error.[76] These models meet this rule.

The mean values of the standard error and the sum of squares of residuals may be obtained from Appendix II:

	Mean S.E.	Mean PHI
Models 1 and 4.	.03832	.010149
Model 2.	.01973	.00222
Model 3.	.01958	.002208

The standard error for Model 2 and 3 is approximately one half of the corresponding error for Models 1 and 4. The sum of the squares of residuals, PHI, for Models 2 and 3 is approximately one-fifth the corresponding error for Models 1 and 4. Hence Models 1 and 4 are rejected as models representing the system. It remains to decide between Models 2 and 3.

An examination of the parameters for Model 2 in Appendix II reveals that eighteen values of k_2 have negative upper and lower confidence limits. Hence Model 2 is rejected on the grounds that the model has a negative parameter which cannot be justified on physical grounds. Furthermore, the negative parameter values are negative in a statistical sense, i.e., they do not become positive over a portion of their confidence intervals.

It is concluded that Model 3 best represents the catalytic reaction of this research. The standard error of Model 3 lies within experimental error as calculated in Appendix III. This model substantiates the assumption made previously, namely, that the chemisorption of oxygen is fast, and hence is not rate controlling.

The values of unreacted $^{*}CO$, $f_{*_{CO}}$, predicted by Model 3 are presented in Table II-6. The temperature was not included as a variable in parameter estimation to increase the number of data points because of convergence difficulties.

C. Results from Mathematical Modeling.

Having established Model 3 as the best model for the process, the temperature dependency of the reaction may be shown to follow the Arrhenius equation. It can be seen that the contribution of the secondary reaction to the consumption of carbon monoxide is negligibly small compared to the corresponding contribution of the primary reaction. With this consideration, only one rate constant, k_1, need be considered. The results of calculations based on the Arrhenius equation,

$$k_1 = k_o(O\text{-}Si_1) \exp(-E/RT) \qquad (32)$$

are tabulated in Table II-5. Arrhenius plots are shown in Figures 15-18. The values of E and k_o' in Table II-4 have been found by the use of Marquardt's program.[65]

The activation energy, E, as a function of the Al_2O_3/MgO ratio is shown in Figure 19. This plot is in the form of a maximum type curve. Within experimental error, it may be predicted that the maximum point occurs at an Al_2O_3/MgO ratio of 1.667. At this value of x, the structural formula of magnesium aluminate is $\left[MgAl_2O_4\right]_1\left[Al_{8/3}\square_{1/3}O_4\right]_{0.5}$, where $\square$ denotes a vacancy.

This maximum type of curve has been reported by

Claudel and Brau[77] for uranium-thorium mixed oxides in carbon monoxide oxidation.

The variable frequency factor k_o' reported in Table II-4 may be written as a function of the number of active oxygen sites,

$$k_o' = k_o(O\text{-}Si_1) \qquad (33)$$

The frequency factor k_o is a true constant; hence the variable frequency factor k_o' is directly proportional to the number of active oxygen sites. Since k_o is a constant, Figure 20 shows how the number of active oxygen sites changes with the Al_2O_3/MgO ratio. The plot is also in the form of a maximum type curve; within experimental error, the maximum point may be predicted to occur at $x = 1.667$.

Examination of Table II-4 reveals that catalysts at different compositions show different values for the activation energy, but high values of activation energy are accompanied by high values of the frequency factor k_o. Due to these compensating changes in the frequency factor, the rate constant k_1 of all the catalysts lie within an order of magnitude. This is the well documented compensation effect.[78] This is interpreted to mean that different parts of the surface area are in action at different compositions, and the relevant heats of adsorption are different.

Figure 5, a plot of the percentage of cation vacancies versus the Al_2O_3/MgO ratio, does not have a maximum point.

A comparision of Figures 19 and 20 with Figure 5 shows that there is no relationship between the percentage of cation vacancies and the activation energy or the number of active sites. Since there is no correlation with the number of cation vacancies, the catalytic activity is not affected by atomic defects of cation vacancies.

In the composition range $1.0 < x < 1.667$, the increase in the number of active sites with increase of alumina content indicates that the active sites for "weak" oxygen adsorption are the normal aluminum lattice cations which are exposed to the surface of the catalyst. The active sites are the octahedral sites in the spinel structure, since Figure 3 (p. 18) indicates that these sites consist of 94% aluminum, whereas the tetrahedral sites consist of only 12% aluminum.

The active sites are affected by the local bulk composition of the catalyst; the composition will determine the polarization charge available at the active site. The activation energy of the oxidation reaction is maximum at the composition $x = 1.667$; hence the adsorption bond formed between oxygen and the active site is strongest at this composition. Consequently, the maximum polarization charge occurs at the composition $x = 1.667$. Deviation from the composition $x = 1.667$ results in a decrease in the strength of the adsorption bond and a corresponding decrease in activation energy.

The normal cation lattice sites were found to be the active sites for the exchange reaction of CO and CO_2 on cobalt ferrite catalysts in the recent works of Huang and Squires.[96]

The growth of single crystal spinel involves the precipitation of spinel from supersaturated solution. It is now established[88] that, in many alloys, precipitation is preceded by the formation of clusters rich in solute atoms within the parent lattice. These segregates retain the structure of the parent phase and are completely coherent in it, although this may produce appreciable elastic strains since the local lattice spacing and the local composition will have different values within a cluster. The clusters may be detected in most crystals by refined X-ray methods or high resolution electron microscopy at an early stage in the reaction, and are generally known as Guiner-Preson zones, after the two

workers who first discovered them.

Guinier-Preston zones sometime form as plates on preferred matrix planes; in other cases the zones form as spherical aggregates surrounded by corresponding spherical shells depleted in solute atoms. The dimensions are small for spherical zones, typically about 50 atom spacings in diameter, and plate-shaped zones are only a few atoms thick.

The formation of G.P. zones is often the first stage in a complex sequence of changes, and may be followed by the precipitation of one or more metastable transition phases. These are solute rich phases of definite composition and structure which are never present in the assembly at equilibrium. A metastable structure is usually coherent with the parent phase over most of the interface, and is frequently precipitated as plates of definite habit plane. The only reason for the formation of a non-equilibrium precipitate must be that it can form more rapidly than the equilibrium phase, even though the latter gives a greater lowering of free energy.[88]

Saalfeld and Jogodzinski[36] reported that alumina-rich spinels form precipitations during the annealing processes and during the annealing that occurs on cooling immediately after growth. They found that, regardless of the excess of alumina, Mg-Al spinels form pre-precipitation nuclei above 600 ^{o}C. In spinels with $x > 2.5$, an

intermediate phase appears above 850 °C. Alpha-Al_2O_3 is exsolved above 1000 °C. in spinels with $x > 1.7$. Pre-precipitation appears only at lower temperatures and disappears as the intermediate phase or alpha-Al_2O_3 forms; the transition is continuous.

Mg-Al alloys are difficult to study by X-ray techniques since the atomic scattering factors of aluminum and magnesium are close. The only evidence for the formation of G.P. zones in Mg-Al alloys is the electrical resistivity results of Federighi.[92] It has not yet been possible to obtain electron diffraction patterns of precipitates in Mg-Al alloys.[92]

Observations by Mehl and Jetter[91] of the striated structures produced on Al-Cu alloys were assumed to result from the formation of Guinier-Preston zones. Wang[6] reported growth striations around the outside edges of stoichiometric magnesium aluminate crystals. The strain associated with these striations is directed along the directions normal to the growth facets. These striations are due to segregation of impurities at the solid-liquid interface during growth. There was no evidence of precipitation of impurities at the solid-liquid interface. Electron diffraction patterns indicated the presence of strain in non-stoichiometric single crystals of magnesium aluminate. Further annealing treatment of these crystals was recommended to reduce the strains.[6] The presence of

growth striations and strains in the magnesium aluminate single crystals is hence interpreted to indicate the possibility of the presence of G.P. zones, particularly since there is no evidence of precipitates.

A number of important properties have been observed about magnesium aluminate with the composition x = 1.7.[79] The mechanical strength of magnesium aluminate is minimum at this composition. Transmission measurements by optical spectroscopy are also minimal at x = 1.7.

Grabmaier and Falckenberg[89] studied Al-rich single crystals of Mg-Al spinels with molar ratios of 1.7 to 3.5 grown by flame fusion. They found that in unannealed crystals the strength increased with increasing alumina content; they also found that strength was influenced by the temperature of heat treatment. The strength increased with increasing annealing temperature above 650 °C. up to a maximum value; the temperature at which this value was reached depended on the molar ratio of the spinel and the duration of annealing. The strengthening found in Mg-Al spinels is thought to be age strengthening as is often observed in alloys.[90] This is inferred because all characteristics of age strengthening are present: (1) The solubility in the solid state increases with decreasing temperature, (2) Strengthening is determined by the first stage of formation of a compound (Guinier-Preston zones),

(3) Strengthening disappears on annealing at high temperatures followed by rapid cooling. Grabmaier and Falckenberg report that Mg-Al spinel is probably the first oxide in which age strengthening has been observed. Hence pre-precipitation is thought to be the cause of the observed strengthening.

The decrease of mechanical strength of magnesium aluminate as the composition increases from $x = 1.0$ to $x = 1.667$, and the increase of mechanical strength as the composition increases from $x = 1.667$ to $x = 3.0$ is attributed to pre-precipitation phenomena. The basis for this correlation is the evidence that mechanical strengthening in alloys is due to pre-precipitation phenomena.

The increase in strength properties due to the presence of small coherent pre-precipitation nuclei clusters is due to the large elastic strain of the lattice immediately adjacent to the clusters. This elastic strain is necessary in order to accomodate all the bonds required of a coherent interface between the matrix and the clusters.[93]

The presence of growth striations in stoichiometric spinels indicates that pre-precipitation nuclei are numerous in stoichiometric spinels. As the composition increases from $x = 1.0$ to $x = 1.667$, the number of

pre-precipitation nuclei apparently decreases; correspondingly, the mechanical strength also decreases. With further increase of composition from x = 1.667 to x = 3.0, the number of pre-precipitation nuclei increases; correspondingly, the mechanical strength also increases.

The behavior of the number of active sites, as illustrated in Figure 20, is related to the number of pre-precipitation nuclei. The nuclei clusters interact with the active sites to effectively block their catalytic activity. As the number of pre-precipitation nuclei increases, the number of active sites which remain available for oxygen adsorption decreases.

The relationship of the activation energy and the number of active sites with the pre-precipitation nuclei explains the observed compensation effect on magnesium aluminate catalysts: different parts of the surface are in action at different compositions.

CHAPTER VI

CONCLUSIONS

The following conclusions may be drawn from the results and discussion in Chapter V.

1. Magnesium aluminate is known to be an insulator; furthermore, its conductivity does not vary with respect to composition, x, in the range 1.0 to 3.0. In contrast, the catalytic activity varies greatly with respect to composition in the same range. Specifically, the activation energy is three times greater at x = 1.7 than at x = 1.0. This finding confirms that there are effects other than mere electronic differences of the catalyst that are affecting the catalytic activity. The results of this research bring into question the Electronic Theory of Catalysis; in this case this theory is unable to account for the catalytic activity of an insulator or the change in catalytic activity with different catalyst composition in which the electron concentration remains constant.

2. The composition of crystal mixture in a single crystal structure is one of the factors which will greatly affect catalytic activity. This has been confirmed by the observed difference in activation energy with composition; the activation energy reached a maximum value when the composition was 1.667. The composition affects the activation energy by influencing the strength of adsorption bond formed between the catalyst and the "weakly" adsorbed

oxygen.

2. The composition of crystal mixture also affects the number of active sites on the magnesium aluminate catalyst. The influence of the composition is to affect the number of pre-precipitation nuclei; the pre-precipitation nuclei inhibit the catalytic activity of the active sites. This accounts for the maximum number of active sites when the composition, x, is 1.667. The basis for determining the number of pre-precipitation nuclei is its known effect on the mechanical strength of alloys. In this case the mechanical strength is minimal at $x = 1.667$.

3. The combined affect of composition on the activation energy and the number of active sites explains the observed compensation effect: different parts of the catalyst surface are in action at different compositions.

4. The active sites for "weak" oxygen adsorption are the normal aluminum lattice cations; these sites are located in octahedral positions of the spinel structure. The basis for this finding is the observed increase in the number of active sites with increasing alumina content in the composition range $1.0 < x < 1.667$.

5. For the catalytic oxidation of carbon monoxide on magnesium aluminate in the temperature range of 500 to 600 ^{o}C., the process proceeds mainly via the reaction of

gaseous CO with chemisorbed oxygen. The oxygen is "weakly" chemisorbed as a boundary layer and not by electron transfer with lattice atoms. A secondary reaction occurs at a much smaller rate than the primary reaction. The secondary reaction proceeds by the reaction of "weakly" chemisorbed CO and oxygen on adjacent sites. The fraction of unreacted radioactive CO, f_{*co}, is given by

$$f_{*co} = ((k_1+k_2)\exp(-k_1 t)-k_2)/k_1$$

6. The catalytic activity is not directly related to the number of cation vacancies. The number of cation vacancies does not correlate with the activation energy or the number of active sites.

7. When carbon monoxide is analyzed by freeze separation from CO_2, a correction must be made for the solubility of carbon monoxide in carbon dioxide.

RECOMMENDATIONS

The following recommendations are made for future work which could evolve from the results of the present work.

1. A more extensive theoretical basis for catalysis should employ solid state physics and quantum mechanics. In their present stage of development, however, these fields consider only the interior of a solid, they are unable to deal with surface type phenomena.

2. Pre-precipitation phenomena has never before been related to catalytic activity, probably because it is difficult to detect by current X-ray and electron microscopy methods. Also, in metals and semi-conductors the electronic properties may appear to be of more importance to catalytic activity. Further study of pre-precipitation phenomena may be very fruitful.

3. Experimental verification of the behavior of pre-precipitation nuclei rests with developments in refining X-ray and electron microscopy techniques.

NOMENCLATURE

COCM	Catalytic oxidation of carbon monoxide.
D_{im}	Diffusivity of i in a mixture, $cm^2/sec.$
f_{*co}	Fraction of unreacted radioactive CO.
ΔF	Free energy change, in cal.
k	Rate constant, $(hr.(m\ gm.\ catalyst))^{-1}$
M	Molecular weight.
m	Mass of catalyst, in grams.
P	Pressure, in atmospheres.
Si	Active site, (no. of active sites/m gm. catalyst)
(O-Si)	Oxygen adsorbed on an active site (no. of active oxygen sites/m gm. catalyst).
(CO-Si)	CO adsorbed on an active site, (no. of active CO sites/m gm. catalyst).
t	Time, in hours.
T	Temperature, in degrees centrigrade.
x	Composition of magnesium aluminate, $MgO:xAl_2O_3$.
*	Denotes radioactive component, when used in *CO.
Φ_L	Thiele modulus, dimensionless.
η	Effectiveness factor, dimensionless.

APPENDIX

APPENDIX I: EXPERIMENTAL DATA.

TABLE I-1.
The Oxidation of Carbon Monoxide catalyzed by 0.300 gm. $MgO:xAl_2O_3$.

Time (hrs.)	Total Counts Per Two Minutes	CO Counts Per Two Minutes	CO%
	Run No. 15-1, x = 3.000, T = 501.5 °C.		
0.0	3788	3480	100.3
2.0	3469	2818	89.6
4.0	3432	2399	77.1
6.5	2611	1510	63.9
9.5	2541	1150	50.1
12.0	2489	1036	46.0
24.0	2956	450	16.8
	Run No. 15-2, x = 3.000, T = 545.1 °C.		
0.0	1853	1725	100.2
1.5	2946	2400	89.97
4.0	2963	2003	74.65
6.0	2923	1577	59.59
8.0	2550	1091	47.3
10.0	2942	950	35.66
12.0	2852	756	29.9
22.5	2417	32	1.47

TABLE I-1.(Continued)

Time (hrs.)	Total Counts Per Two Minutes	CO Count Per Two Minutes	CO%
	Run No. 15-3, x = 3.000, T = 575 °C.		
0.0	2735	2484	100.3
2.0	3809	2722	78.7
4.0	3926	2015	56.6
5.0	2937	1411	53.1
7.0	3070	1044	37.5
9.0	2723	583	23.7
11.0	2837	399	15.5
	Run No. 15-4, x = 3.000, T = 597.9 °C.		
0.0	2463	2244	100.8
2.0	5056	3206	69.8
4.0	3507	1664	52.3
5.0	3257	1023	34.6
7.0	3321	761	25.3
9.0	2767	260	10.4
11.0	2795	42	1.66

TABLE I-1 (Continued)

Time (hrs.)	Total Counts Per Two Minutes	CO Counts Per Two Minutes	CO%
	Run No. 16-1, x = 2.500, T = 502.5 °C.		
0.0	2350	2152	101.3
2.0	4350	3515	89.0
4.0	3704	2776	82.6
6.0	3980	2801	77.6
8.0	3550	2223	69.1
10.0	3750	1966	57.8
14.0	3231	1277	43.6
26.0	3410	451	14.6
	Run No. 16-2, x = 2.500, T = 549.8 °C.		
0.0	4957	4563	101.3
1.0	4213	3460	90.5
2.0	4448	3288	81.4
4.0	3693	2072	61.9
6.0	3339	1317	43.5
8.0	3356	798	26.2
10.0	3113	399	14.1

TABLE I-1. (Continued)

Time (hrs.)	Total Counts Per Two Minutes	CO Counts Per Two Minutes	CO%
	Run No. 16-3, x = 2.500, T = 579.4 °C.		
0.0	3668	3435	103.2
1.17	3639	2621	79.4
2.0	3619	2050	62.46
3.0	3635	1582	47.9
4.0	3837	1064	30.6
5.35	3905	520	14.7
6.53	3087	93	3.3
	Run No. 16-4, x = 2.500, T = 604.5 °C.		
0.0	4049	3686	101.8
1.067	3832	2294	65.9
2.05	3932	1419	39.8
3.83	3685	601	17.9
4.83	3629	95	2.8

TABLE I-1.(Continued)

Time (hrs.)	Total Counts Per Two Minutes	CO Count Per Two Minutes	CO%
	Run No. 17-1, x = 1.700, T = 499.7 °C.		
0.0	4074	3764	101.8
2.167	3040	2628	95.5
4.0	3788	2969	86.4
7.0	3195	2250	77.2
10.0	3620	2330	70.9
12.0	3549	2166	67.3
23.5	3475	1281	40.7
	Run No. 17-2, x = 1.700, T = 554.4 °C.		
0.0	3946	3595	100.4
1.0	4064	3404	92.3
3.0	4109	2910	78.0
6.5	3351	1698	55.9
9.0	4008	1445	39.7
12.0	3454	883	28.2
24.0	3508	241	7.5

TABLE I-1.(Continued)

Time (hrs.)	Total Counts Per Two Minutes	CO Counts Per Two Minutes	CO%
	Run No. 17-3, x = 1.700, T = 575.0 °C.		
0.0	4409	3986	99.6
1.0	4141	2879	76.6
2.0	3687	2328	69.6
3.03	3049	1717	62.2
5.0	3417	1252	40.2
7.0	3296	761	25.5
9.0	3040	407	14.8
	Run No. 17-4, x = 1.700, T = 601.8 °C.		
0.0	3996	3698	101.9
1.0	4075	2549	68.9
2.0	4023	1743	47.7
3.08	3452	1233	39.4
4.72	3616	713	21.7
5.5	3070	410	14.7
6.5	3267	257	8.7

TABLE I-1.(Continued)

Time (hrs.)	Total Counts Per Two Minutes	CO Counts Per Two Minutes	CO%
	Run No. 18-1, x = 1.500, T = 507.3 °C.		
0.0	4345	4039	102.3
2.5	4325	3566	90.8
5.0	4064	3003	81.4
7.0	3943	2532	70.7
10.0	3545	1980	61.6
12.0	3390	1719	55.9
25.5	3218	787	26.9
	Run No. 18-2, x = 1.500, T = 549.1 °C.		
0.0	4584	4206	101.0
2.22	4050	2991.	81.4
4.63	4496	2340	57.3
6.46	4629	2070	49.2
8.05	4324	1585	40.4
12.0	4857	1087	24.6
27.63	1091	80	8.2

TABLE I-1.(Continued)

Time (hrs.)	Total Counts Per Two Minutes	CO Counts Per Two Minutes	CO%
	Run No. 18-3, x = 1.500, T = 579.0 °C.		
0.0	4862	4585	103.8
1.0	4036	3103	84.7
2.28	4020	2378	65.2
3.0	4246	2108	54.7
4.0	4617	1810	43.2
6.5	3450	831	26.6
8.0	3346	500	16.5
	Run No. 18-4, x = 1.500, T = 601.4 °C		
0.0	4521	4125	100.4
1.0	4413	2439	60.9
2.16	4235	1272	33.1
3.83	4258	919	23.7
4.0	3561	610	18.9
5.75	3100	170	6.1

TABLE I-1.(Continued)

Time (hrs.)	Total Counts Per Two Minutes	CO Counts Per Two Minutes	CO%
	Run No. 19-1, x = 1.000, T = 500.5 °C.		
0.0	3522	3243	101.5
1.0	3368	2907	95.2
3.5	3784	2560	74.6
5.5	3754	2143	62.9
7.5	3689	1722	51.5
9.5	3252	1256	42.6
12.0	3034	892	32.5
	Run No. 19-2, x = 1.000, T = 546.8 °C.		
0.0	4476	4125	101.5
2.0	4496	3091	75.7
3.0	4055	2380	64.7
4.0	3419	1706	55.0
6.0	3249	1177	39.9
8.0	3157	741	25.9
11.0	2974	347	12.8

TABLE I-1.(Continued)

Time (hrs.)	Total Counts Per Two Minutes	CO Counts Per Two Minutes	CO%
	Run No. 19-3, x = 1.000, T = 577.9 °C.		
0.0	4534	4178	101.5
1.0	4352	3244	82.1
2.0	4000	2354	64.8
3.0	4185	1822	47.9
4.0	3341	1165	38.9
5.5	3335	646	21.4
7.0	3343	320	10.6
	Run No. 19-4, x = 1.000, T = 599.6 °C.		
0.0	3918	3633	102.2
1.0	3327	2255	74.8
2.0	3213	1666	57.2
3.0	3342	1233	40.7
4.0	3145	765	26.8
5.0	2736	343	13.8
6.0	2858	88	3.4

APPENDIX II. THEORETICAL DATA.

TABLE II-1.
Parameter Information for Models 1 and 4.

Al_2O_3/MgO	Temp.,°C.	k_1	95% Confidence Intervals	S.E.	PHI
1.0	500.5	.0885	.0836< x <.0933	.0201	.00242
	546.8	.1577	.1464< x <.1688	.0277	.00462
	577.9	.2511	.2241< x <.2781	.0417	.01045
	599.6	.3332	.2846< x <.3817	.0566	.01925
1.5	507.3	.0485	.0456< x <.0514	.0197	.00234
	549.1	.1117	.1045< x <.1189	.0236	.00335
	579.0	.2039	.1899< x <.2179	.0261	.00409
	601.4	.4762	.4443< x <.5079	.0223	.00250
1.7	499.7	.0357	.0332< x <.0382	.0201	.00242
	554.4	.0982	.0911< x <.1052	.0251	.00378
	575.0	.2891	.2353< x <.3429	.0421	.01064
	601.8	.5010	.3947< x <.6073	.0299	.00539
2.5	502.5	.0561	.0488< x <.0633	.0468	.01536
	549.8	.1465	.1231< x <.1699	.0592	.02103
	579.4	.2891	.2353< x <.3429	.0730	.03198
	604.5	.5010	.3947< x <.6073	.0681	.01853
3.0	501.5	.0689	.0650< x <.0728	.0197	.00234
	545.1	.0966	.0842< x <.1089	.0490	.01441
	573.9	.1442	.1299< x <.1586	.0398	.00948
	597.9	.2384	.2046< x <.2723	.0557	.01861

Note: $x = k_1$ above. Dimensions of $k_1 = ((hr.)(.3\ gm.\ catalyst))^{-1}$.

TABLE II-2.
Parameter Information for Model 2.

Al_2O_3/MgO	Temp.,°C.	k_1	k_2	S.E.	PHI
1.0	500.5	.0789	-.02007	.0151	.00114
	546.8	.1388	-.02618	.0087	.00038
	577.9	.2065	-.05825	.0149	.00114
	599.9	.2529	-.0872	.0139	.00096
1.5	507.3	.0456	-.00609	.0174	.00152
	549.1	.1153	.00458	.0222	.00245
	579.0	.1883	-.0217	.0226	.00255
	601.4	.4975	.1651	.0223	.00200
1.7	499.7	.0324	-.0097	.0173	.00150
	554.4	.0934	-.00587	.0225	.00255
	575.0	.1688	-.0231	.0415	.00864
	601.8	.3354	-.00300	.0327	.00537
2.5	502.5	.0463	-.0188	.0227	.00309
	549.8	.1033	-.0681	.0134	.00091
	579.4	.2076	-.1008	.0191	.00183
	604.5	.3665	-.1396	.0122	.00045
3.0	501.5	.0657	-.0051	.0182	.00166
	545.1	.0679	-.0577	.0116	.00068
	573.9	.1218	-.0312	.0279	.00392
	597.9	.1919	-.0483	.0184	.00169

Note: Dimensions of k_1, k_2 = $((hr.)(.3\ gm.\ catalyst))^{-1}$.

TABLE II-2.(Continued)
Parameter Information for Model 2.

Al_2O_3/MgO	Temp.,°C.	95.0% Confidence Intervals	
		$k_1 = x$	$k_2 = y$
1.0	500.5	.0669< x <.0907	-.0436< y< .00342
	546.8	.1309< x <.1467	-.0354< y<-.01695
	577.9	.1856< x <.2275	-.0822< y<-.0343
	599.6	.2294< x <.2764	-.1105< y<-.0639
1.5	507.3	.3966< x <.0516	-.0164< y<-.00418
	549.1	.1024< x <.1282	-.0055< y< .01474
	579.0	.1588< x <.2177	-.0563< y< .01288
	601.4	.4201< x <.5751	.0309< y< .06396
1.7	499.7	.0267< x <.0382	-.0249< y< .00545
	554.4	.0812< x <.1056	-.0164< y< .00462
	575.0	.1184< x <.2192	-.8038< y< .03418
	601.8	.2606< x <.4102	-.5755< y< .05155
2.5	502.5	.0396< x <.0531	-.0289< y<-.00882
	549.8	.0919< x <.1148	-.0855< y<-.05066
	579.4	.1817< x <.2336	-.1297< y<-.07195
	604.5	.3313< x <.4017	-.1728< y<-.10654
3.0	501.5	.0579< x <.0735	-.0148< y< .00472
	545.1	.0604< x <.0754	-.0731< y<-.04238
	573.6	.0971< x <.1467	-.0627< y<-.000298
	597.9	.1713< x <.2126	-.0661< y<-.03058

Note: Dimensions of k_1, k_2 = $((hr.)(.3\ gm.\ catalyst))^{-1}$.

TABLE II-3.
Parameter Information for Model 3.

Al_2O_3/MgO	Temp., °C.	k_1	k_2	S.E.	PHI
1.0	500,5	.0587	.02007	.0151	.001137
	546.8	.1126	.02618	.0056	.000158
	577.9	.1483	.05826	.0146	.00111
	599.9	.1657	.0872	.0139	.000969
1.5	507.3	.0395	.00609	.0174	.001516
	549.1	.1198	-.00459	.0222	.00245
	579.0	.1665	.02172	.0226	.00255
	601.8	.5141	-.01651	.0224	.00200
1.7	499.7	.0227	.00975	.0173	.00150
	554.4	.0875	.00587	.0226	.00255
	575.0	.1457	.02309	.0416	.00863
	601.8	.3324	.00330	.0327	.00537
2.5	502.5	.0274	.01889	.0227	.003089
	549.8	.0353	.06811	.0135	.000908
	579.4	.1069	.1008	.0191	.001833
	604.5	.2268	.1396	.0122	.000448
3.0	501.5	.0607	.00506	.0182	.001662
	545.1	.0625	.05773	.0116	.000676
	573.9	.0907	.03120	.0279	.003919
	597.9	.1436	.04833	.0184	.001698

Note: Dimensions of $k_1 = ((\text{hr.})(.3 \text{ gm. catalyst}))^{-1}$

$k_2 = \text{atm.}/((\text{hr.})(.3 \text{ gm. catalyst}))$

TABLE II-3.(Continued)
Parameter Information for Model 3.

Al_2O_3/MgO	Temp.,°C.	95.0% Confidence Intervals	
		$k_1 = x$	$k_2 = y$
1.0	500.5	.0240< x <.0935	-.00342< y <.0435
	546.8	.1021< x <.1232	.02025< y <.0321
	577.9	.1050< x <.1916	.03430< y <.0822
	599.9	.1204< x <.2110	.06393< y <.1105
1.5	507.3	.0239< x <.0551	-.00418< y <.0163
	549.1	.0990< x <.1407	-.01474< y <.0055
	579.0	.1049< x <.2281	-.01288< y <.0563
	601.4	.3955< x <.6326	-.06396< y <.0309
1.7	499.7	.0022< x <.0432	-.00545< y <.0249
	554.4	.0664< x <.1085	-.00462< y <.0163
	575.0	.0419< x <.2495	-.03418< y <.0804
	601.8	.2085< x <.4564	-.05155< y <.0575
2.5	502.5	.1145< x <.0434	.00882< y <.0289
	549.8	.0069< x <.0635	.05066< y <.0855
	579.4	.0538< x <.1598	.07195< y <.1296
	604.5	.1608< x <.2929	.10654< y <.0727
3.0	501.5	.0441< x <.0774	-.00472< y <.0148
	545.1	.0442< x <.0809	.01005< y <.0297
	573.6	.0359< x <.1454	-.00029< y <.0627
	597.9	.1069< x <.1803	.30583< y <.0661

Note: Dimensions for k_1 and k_2 are given on the previous page.

TABLE II-4

Activation Energy and Frequency Factor

Values Predicted by Model 3.

Al_2O_3/MgO	Activation Energy, E (cal/mole)	Frequency Factor, k'_o
1.0	14,267.08	661.48
1.5	34,121.02	1.3399×10^8
1.7	34,572.75	1.2909×10^8
2.5	28,033.16	1.6644×10^6
3.0	11,388.72	86.48

Note: Dimensions of $k'_o = ((\text{hr.})(.3 \text{ gm. catalyst}))^{-1}$.

TABLE II-5.

Predicted Values of f^*_{co} by Model 3.

$Al_2O_3/MgO = 1.0$

Time (hrs.)	F Obs.	F Pred.	F Diff.
T = 500.5 °C.			
0.0	1.0150	1.0000	.01499
1.0	.9522	.9234	.02879
3.5	.7460	.7505	-.00452
5.5	.6290	.6294	-.00038
7.5	.5146	.5217	-.00708
9.5	.4260	.4259	.000065
12.5	.3246	.3210	.00355
T = 546.8 °C.			
0.0	1.0000	1.0000	-.931E-09
2.0	.7570	.7514	.00558
3.0	.6467	.6466	.882E-04
4.0	.5504	.5529	-.00257
6.0	.3990	.3945	.00445
8.0	.2590	.2680	-.00908
11.0	.1288	.1246	.00423
T = 577.9 °C.			
0.0	1.0147	1.0000	.0147
1.0	.8210	.8079	.0130
2.0	.6485	.6425	.0060
3.0	.4796	.4997	-.0202
4.0	.3897	.3767	.0129
5.5	.2137	.2232	-.0095
7.0	.1056	.1003	.0053

Note: F represents the computer symbol for f^*_{co}.

TABLE II- 5.(Continued)

$Al_2O_3/MgO = 1.0$

Time (hrs.)	F Obs.	F Pred.	F Diff.
T = 599.6 °C.			
0.0	1.0220	1.0000	.02199
1.0	.7478	.7669	-.01910
2.0	.5720	.5694	.00259
3.0	.4070	.4021	.00493
4.0	.2685	.2603	.00820
5.0	.1385	.1402	-.00168
6.0	.0340	.0384	-.00440

$Al_2O_3/MgO = 1.5$

T = 507.3 °C.			
0.0	1.0230	1.0000	.02299
2.5	.9081	.8914	.01673
5.0	.8142	.7929	.02124
7.0	.7077	.7209	-.01324
10.0	.6159	.6231	-.00715
12.0	.5594	.5639	-.00456
25.5	.2699	.2669	.00296
T = 549.1 °C.			
0.0	1.0100	1.0000	.00999
2.217	.8137	.7755	.03818
4.63	.5731	.5903	-.01721
6.46	.4923	.4815	.01075
8.05	.4037	.4046	-.00091
12.0	.2463	.2664	-.02011
27.63	.0822	.0733	.00886

TABLE II-5. (Continued)

$Al_2O_3/MgO = 1.5$

T = 579.0 °C.

Time (hrs.)	F Obs.	F Pred.	F Diff.
0.0	1.038	1.0000	.03799
1.0	.8472	.8266	.02062
2.28	.6518	.6428	.00894
3.0	.5469	.5554	-.00858
4.0	.4316	.4503	-.01866
6.5	.2657	.2525	.01318
8.0	.1648	.1679	-.00306

T = 601.8 °C.

0.0	1.0040	1.0000	.00399
1.0	.6087	.6109	-.00225
2.167	.3308	.3498	-.01900
3.083	.2377	.2305	.00721
4.0	.1889	.1559	.03297
5.75	.0605	.0825	-.02196

$Al_2O_3/MgO = 1.7$

T = 499.7 °C.

0.0	1.0180	1.0000	.01800
2.167	.9545	.9313	.02315
4.0	.8640	.8759	-.01185
7.0	.7726	.7899	-.01728
10.0	.7097	.7096	.00014
12.0	.6730	.6590	.01402
23.5	.4066	.4088	-.00221

TABLE II-5.(Continued)

$Al_2O_3/MgO = 1.7$

Time (hrs.)	F Obs.	F Pred.	F Diff.
T = 554.4 °C.			
0.0	1.0040	1.0000	.00399
1.0	.9229	.9106	.01230
3.0	.7803	.7536	.02666
6.5	.5590	.5371	.02187
9.0	.3972	.4184	-.02120
12.0	.2819	.3063	-.02440
24.0	.7577	.0635	.01224
T = 575.0 °C.			
0.0	.9956	1.0000	-.00440
1.0	.7659	.8429	-.07699
2.0	.6960	.7071	-.01110
3.167	.6217	.5717	.04997
5.0	.4042	.4005	.00365
7.0	.2547	.2592	-.00450
9.0	.1478	.1536	-.00579
T = 601.8 °C.			
0.0	1.0190	1.0000	.01899
1.0	.6892	.7146	-.02543
2.0	.4774	.5099	-.03256
3.167	.3940	.3431	.05092
4.717	.2174	.2013	.01609
5.5	.1474	.1531	-.00570
6.5	.0868	.1073	-.02045

TABLE II-5.(Continued)

$Al_2O_3/MgO = 2.5$

Time (hrs.)	F Obs.	F Pred.	F Diff.
T = 502.5 °C.			
0.0	1.0130	1.0000	.01299
2.0	.8900	.9098	-.01983
4.0	.8260	.8245	.00152
6.0	.7755	.7437	.03182
8.0	.6905	.6672	.02329
10.0	.5779	.5948	-.01690
14.0	.4362	.4614	-.02520
26.0	.1458	.1388	.00701
T = 549.8 °C.			
0.0	1.0130	1.0000	.01299
1.0	.9047	.8984	.00627
2.0	.8140	.8003	.01362
4.0	.6186	.6144	.00425
6.0	.4350	.4409	-.00598
8.0	.2620	.2794	-.01743
10.0	.1414	.1288	.01253
T = 579.4 °C.			
0.0	1.0320	1.0000	.03199
1.117	.7940	.7813	.01267
2.0	.6246	.6260	-.00142
3.0	.4799	.4669	.01295
4.0	.3056	.3240	-.01841
5.35	.1467	.1537	-.00705
6.53	.0333	.0237	.00949

TABLE II-5.(Continued)

$Al_2O_3/MgO = 2.5$

Time (hrs.)	F Obs.	F Pred.	F Diff.
T = 604.5 °C.			
0.0	1.0180	1.0000	.01799
1.066	.6598	.6529	.00684
2.05	.3977	.3992	-.00146
3.083	.1798	.1872	-.00737
4.083	.0288	.0243	.00461

$Al_2O_3/MgO = 3.0$

T = 501.5 °C.			
0.0	1.0127	1.0000	.01269
2.0	.8960	.8761	.01988
4.0	.7710	.7664	.00461
6.5	.6394	.6467	-.00731
9.5	.5005	.5251	-.02463
12.0	4600	.4394	.02056
24.0	.1680	.1689	-.00095
T = 545.1 °C.			
0.0	1.0200	1.0000	.01999
1.5	.8997	.8819	.01771
4.0	.7465	.7083	.03819
6.0	.5959	.5877	.00824
8.0	.4730	.4812	-.00819
10.0	.3570	.3872	-.03024
12.0	.2990	.3043	-.00533
22.5	.1470	.0048	.00990

TABLE II-5. (Continued)

$Al_2O_3/MgO = 3.0$

Time (hrs.)	F Obs.	F Pred.	F Diff.
T = 573.9 °C			
0.0	1.0500	1.0000	.04999
2.0	.787	.7770	.00996
4.0	.5640	.5911	-.02705
5.0	.5290	.5099	.01902
7.0	.3760	.3683	.00769
9.0	.2380	.2501	-.01213
11.0	.1560	.1516	.00443
T = 597.9 °C.			
0.0	.9975	1.0000	-.00250
2.0	.6960	.6663	.02971
3.0	.5240	.5321	-.00812
4.5	.3460	.3638	-.01776
5.5	.2790	.2701	.00892
7.5	.1040	.1186	-.01462
9.5	.0166	.0049	.01162

APPENDIX III. ANALYSIS OF ERROR

Experimental Error.

Ten readings from the proportional counter are given to determine the probable error in each count of radioactivity.

n	$n - \bar{n}$	$(n - \bar{n})^2$
5604	+98	9604
5556	+50	2500
5437	-69	4761
5393	-113	12769
5428	-78	6084
5608	+102	10404
5475	-31	961
5461	-45	2025
5610	+104	10816
5486	-20	400

Avg.=5506 Sum=60324

The sample variance, s^2,

$$s^2 = (1/(n-1)) \sum (n-\bar{n})^2 = 60324/9 = 6702.26$$

The sample standard deviation, s,

$$s = \text{SQRT}((1/(n-1)) \quad (n-\bar{n})^2) = \text{SQRT}(6702.66)$$

$$= 81.9$$

The probable error, P,

$$P = 0.6475 \; s = 0.6475(81.9) = 55.24$$

The probable % error $= 100P/\bar{n} = 100(55.24)/5506$

$$= 1.003$$

The background count was approximately 80 counts per minute. When the sample counting rate is below 3000 counts

per minute, the standard deviation due to the background must also be taken into consideration. Above that counting rate, the uncertainty in the background becomes insignificant statistically and may be ignored.(80)

In this research, the counting rate varied from approximately 4500 counts/2 minutes to 25 counts/2 minutes, the counting rate decreasing with reaction. As a result, the background error becomes significant as experimental time increases.

At a gross counting rate of about 100 counts per minute, each count by which the background (70 counts per minute) is incorrect contributes an error to the net sample counts of about 3 %.(81) The background count cannot be counted simultaneously with the sample, on the same counter and in the same counting tube. As a result, some uncertainty in the background count is inevitable. It was observed that the background count may vary 1 to 2 counts per minute from hour to hour and about 3 to 4 counts per minute in a day. Occasionally a variation of as much as 10 counts per minute was observed with one hour counts taken on different days.

In conclusion, it may be assumed that the largest error in the counting rate will occur at low count rates. The count rate decreases with reaction; the total error in

these low count rates, considering background error, will be as high as 4%.

The error in the experimentally calculated values of $f_{*_{CO}}$ may now be calculated.

$$f_{*_{CO}} = Z/X$$

where Z = $^{*}CO$ count after reaction and freeze separation.

X = Corrected *CO count, after reaction, before freeze separation.

$$f_{*_{CO}} = 1.0952\ Z/(Y-24.67)$$

$$df_{*_{CO}} = \frac{1.0952(YdZ-ZdY)-27.013dZ}{(Y-24.67)^2}$$

For small errors in Y and Z the errors in $f_{*_{CO}}$ may be approximated by finite differences,

$$\Delta f_{*_{CO}} = \frac{1.0952(Y\Delta Z-Z\Delta Y)-27.013\Delta Z}{(Y-24.67)^2}$$

For the same error in Y and Z, this reduces to

$$\Delta f_{*_{CO}} = -\frac{27.013\ \Delta Z}{(Y-24.67)^2}$$

Example Calculation.

$Al_2O_3/MgO = 1.0$

Time = 11 hrs.

Y = 2795

Z = 42

Assume that the error in Y and Z both = 4%.

$$f_{*co} = \frac{-27.013(.04)}{(2795-24.67)^2} = -.00039$$

$$f_{*co} = \frac{1.095(42)}{(2795-24.67)} = .0166$$

$$\% \text{ error in } f_{*co} = \frac{.00039(100)}{.0166} = 2.35$$

The formula for f_{*co} has the advantage that a 4% error in its functions Z and X results in an error for f_{*co} that is approximately one half the error of the functions.

The errors for the temperature controller were within $\pm 3\ ^{o}C.$ at $600\ ^{o}C.$

The experimental error in the Arrhenius approximation of the rate constant, k_1, due to the experimental error in the measurement of the temperature may be calculated,

$$k_1 = k_o \exp(-E/RT)$$

$$dk_1 = k_1(E/(RT^2))dT$$

For small errors in Y and Z the errors in k_1 may be approximated by finite differences,

$$\Delta k_1 = k_1(E/(RT^2))\Delta T$$

Example calculation.

$$Al_2O_3/MgO = 1.0$$

$$E = 14{,}593.68 \text{ cal/mole}$$

$$k_1 = .1657$$

$$k_1 = (14{,}593.68)/(1.987*873^2))(.1657)(3)$$

$$= .00479$$

$$\% \text{ error in } k_1 = (.00479)(100)/(.1657) = 2.89$$

The small error in k_1 results mainly because k_1 is small.

The standard error (SE) of the slope E/R in the Arrhenius plots (Figures 15-18) is given by (95)

$$SE = SQRT(\sum(\ln k_{1i} - \ln \bar{k}_1)/(n-2))/SQRT(\sum(X_i - \bar{X}))$$

where X in this case is 1/T, and the bar denotes the average value.

The standard error of the intercept k_o' in the Arrhenius plots is given by (95)

$$SE = SQRT(\sum X_i^2/(n\sum(X_i - \bar{X})^2))*SQRT(\sum(\ln k_{1i} - \ln \bar{k}_1)/(n-2))$$

The calculated maximum value of the standard error is 3210 kcal/gm. mole ($Al_2O_3/MgO = 3.0$); the corresponding standard error for k_o' is 1.95 $((hr.)/(.3\ gm.\ catalyst))^{-1}$. These values for maximum standard error represent percentage errors (for $Al_2O_3/MgO = 3.0$) of 28.2% and 2.26%, respectively.

In Table II-3, the standard error, SE, is given by

$$SE = SQRT(\hat{\Phi}/(n-k))$$

where $\hat{\Phi}$ is the sum of squares of residuals, n is the number of data points, and k is the number of parameters. In Table II-3, SE is a large percentage (maximum 29%) of k_1. The reason for this is that the number of data points, n, is small (seven). This was unavoidable; increasing the number of data points would seriously increase experimental error. (Error in volume of reactor gas).

APPENDIX IV.

Calculation of the Diffusion Rate and Reaction Rate.

I. Molecular Diffusion.

The diffusivity of CO in the mixture $CO-CO_2-O_2$, with mole fractions .25, .50, and .25, respectively, will first be calculated by use of the equation[82]

$$D_{im} = (1-Y_1)/[\sum_{j=2}^{n}(Y_1/D_{1j})] \qquad (1)$$

This equation necessitates calculation of the diffusivities of binary mixtures. The diffusivity of binary mixtures may be calculated from the equation[82]

$$D_{12} = \frac{.001858T^{3/2}[(M_1+M_2)/M_1M_2]^{1/2}}{P\sigma_{12}^2\Omega_D} \qquad (2)$$

Where T = absolute temperature (°K)

M_1, M_2 = molecular weight of the two species.

P = total pressure (atm.)

Ω_D = "collision integral", a function of kT/ε_{12}. (Obtained from tables[ ]).

ε, σ = force constants in the Lennard-Jones potential function.

k = Boltzmann constant.

Binary force constants are obtained by the relationships[82]

$$\varepsilon_{12}/k = \text{SQRT}((\varepsilon_1/k)(\varepsilon_2/k)) \quad (3)$$

$$\sigma_{12} = (1/2)(\sigma_1+\sigma_2) \quad (4)$$

The pertinent data for the $CO-CO_2-O_2$ system is:[82]

No.	Component	ε/k, (°K)	MW	σ, Å
1	CO	110	28	3.590
2	CO_2	190	44	3.996
3	O_2	113	16	3.433

Sample Calculations at 9 mm. Hg. and 500 °C.:

$$\varepsilon_{12}/k = \text{SQRT}(110*190) = 144.57$$

$$\sigma_{12} = (1/2)(3.59+3.996) = 3.793$$

$$kT/\varepsilon_{12} = 773/144.57 = 5.347$$

$$\Omega_D = .8333 \quad [\text{Table, [ ]}]$$

$$\text{SQRT}((M_1+M_2)/M_1M_2) = ((28+44)/28*44))^{1/2}$$

$$= .2417$$

$$D_{12} = \frac{.001858*21491.62*.2417}{.01184*3.793^2*.8333} = 67.99 \text{ cm}^2/\text{sec.}$$

Similar calculations for the binary pair $CO-O_2$ leads to

$$D_{13} = 108.525 \text{ cm}^2/\text{sec.}$$

The diffusivity of CO in the ternary mixture is calculated from Equation 1,

$$D_{co-m} = (1-.25)/((.50/67.99)+(.25/108.525))$$
$$= 77.72 \text{ cm}^2/\text{sec.}$$

This is a notably high diffusivity and results mainly because of the low pressure.

The flux of CO through the gas film boundary layer on the catalyst surface just after time zero is given by

$$N_{co} = -D_{co-m}(dC_{co}/dr) \qquad \text{(gm. moles/(cm.}^2\text{hr.))} \quad (5)$$

where C_{co} = concentration of radioactive carbon monoxide, in (gm. moles/cm.^{3}).

r = radial direction in the reactor, in cm.

It is assumed that diffusion occurs only in the radial direction. This should be a reasonable assumption at low pressures.

The flux may be approximated by using finite difference approximations for the differentials,

$$N_{co} = -D_{co-m}((C_s-C_b)/\delta) \qquad \text{(gm. moles/(cm.}^2\text{hr.))} \quad (6)$$

where C_s = concentration of CO at the solid surface, in (gm. moles/cm.^{3}).

δ = gas film thickness.

The concentration of CO at the solid surface will be negligibly small compared to the concentration of CO in the gas bulk phase, so that the flux equation becomes

$$N_{co} = -D_{co-m}C_b/\delta \qquad \text{(gm. moles/cm.}^2\text{hr.)} \quad (7)$$

The rate of disappearance of CO by diffusion is given by

$$r_D = (N_{co})(A) \quad \frac{\text{(gm. moles)}}{\text{(hr.)(m gm. catalyst)}} \quad (8)$$

where $A = \frac{\text{Outer surface area of catalyst exposed to gas.}}{\text{m gm. catalyst}}$

$$r_D = D_{co\text{-}m} C_{co} A/\delta \qquad (9)$$

It is clear from Eqn. (9) that a small film thickness is most desirable because this will give a large diffusion rate. With this in mind, consider the largest film thickness that is possible - this thickness would correspond to the radius of the reactor in which the catalyst is contained. By utilizing the largest film thickness possible, it is assured that the diffusion rate will not be over-estimated by errors in approximating the film thickness. The diffusion rate may be calculated,

$$r_D = \frac{(279{,}792 \text{ cm}^2/\text{hr})(8 \text{ cm}^2/.3 \text{ gm. catalyst})C_{co}}{(7.62 \text{ cm.})}$$

$$= 293{,}744\ C_{co} \quad (\text{gm. moles}/(\text{hr.}^* \text{ m gm. catalyst})) \qquad (10)$$

Note that the diffusion rate is based on the outer surface area of catalyst bed exposed to the bulk gas phase. This plane surface will be used as a reference to compare the diffusion rate with the surface reaction rate.

2. Pore Diffusion.

The catalyst may be considered to be a flat plate of thickness L, sealed on one side and on the ends. The effective diffusivity, $D_{im,eff}$, of CO in the mixture will be approximated by means of a graph[83] shown in Fig. 21. On this graph $D_{12,eff}/D_{12}$ is correlated with porosity for the diffusion of a hydrogen-air mixture in various porous media.

The use of Figure 21 necessitates the comparision of diffusivities for a hydrogen-air mixture with a $CO-CO_2-O_2$ mixture. The diffusivity of hydrogen-air mixtures is calculated in the same manner as was done for the $CO-CO_2-O_2$ system. The result is

$$D_{12} = 381.8 \text{ cm}^2/\text{sec.}(H_2\text{-air}, T=773 \text{ °K}, P=9 \text{ mm Hg})$$

The catalyst used in this research was finely powered. A conservative estimate for porosity would be .5 cm^3/cm^3. From Figure 21, $D_{12,eff}/D_{12} = .3$

Hence, $$D_{12,eff} = .3*381.8 = 114.54 \text{ cm}^2/\text{sec.}$$

The effective diffusivity of CO in the $CO-CO_2-O_2$ mixture is

$$D_{im,eff} = (77.72/381.8)*114.54$$
$$= 23.316 \text{ cm}^2/\text{sec.}$$

For a first order reaction the Thiele Modulus is defined as[84]

$$\phi_L = L*SQRT[k_v/D_{eff}]$$

The reaction rate constant in this research was of the order of magnitude

$$k_v = .1 \quad [hr]^{-1}$$

Hence, $$\phi_L = (.5 \text{ cm.})*SQRT(.1/(23.316*3600))$$
$$= .00108$$

For a flat plate catalyst with first order reaction,

the effectiveness factor, η, is given by[84]

$$\eta = \tanh\phi_L/\phi_L$$

$$\eta = \tanh(.00108)/.00108$$

$$\eta = 1.0$$

Since the effectiveness factor, η, is defined as the actual rate of reaction in porous catalysts divided by the rate of reaction which would occur if the pellet interior were all exposed to reactants at the same concentration and temperature as that existing at the outside surface of pellet, an effectiveness factor of 1.0 signifies that pore diffusion has no effect in this system.

3. Reaction Rate.

The rate of reaction is given by

$$r_{rxn} = -dn_{co}/mdt = k_f P_{co}$$
$$= k_f RTC_{co}$$

The rate constant in this research was of the order of magnitude

$$k_f = .1 \text{ [hr.(.3 gm. catalyst)]}^{-1}$$

Hence,

$$r_{rxn} = (.1)(82.06)(773)C_{co}$$
$$= 6343\ C_{co} \qquad (11)$$

Divide Eqn. (10) by Eqn. (11) to compare the diffusion rate with the reaction rate:

$$r_D/r_{rxn} = 46 \qquad (12)$$

The rate of diffusion is approximately 46 times greater

than the rate of reaction. This is a conservative minimum estimate.

In summary, the resistances due to pore diffusion have been shown to be negligible. The rate of reaction is negligibly small compared to the rate of diffusion

It is concluded that the rate of reaction is controlling the reaction process because it is much slower than the rate of diffusion.

APPENDIX V

FIGURES 10 - 21.

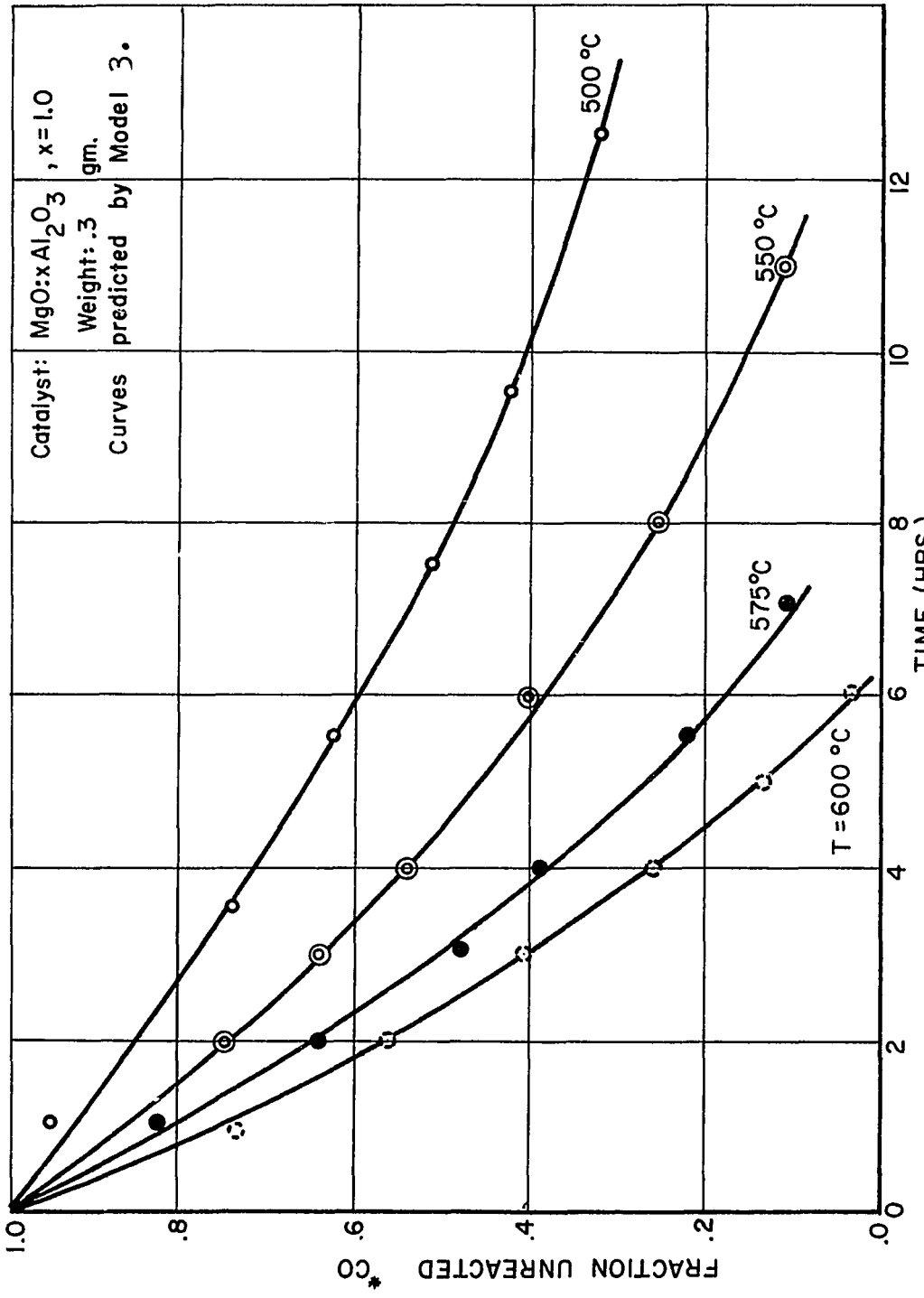

FIGURE 10. FRACTION UNREACTED *CO VERSUS TIME.

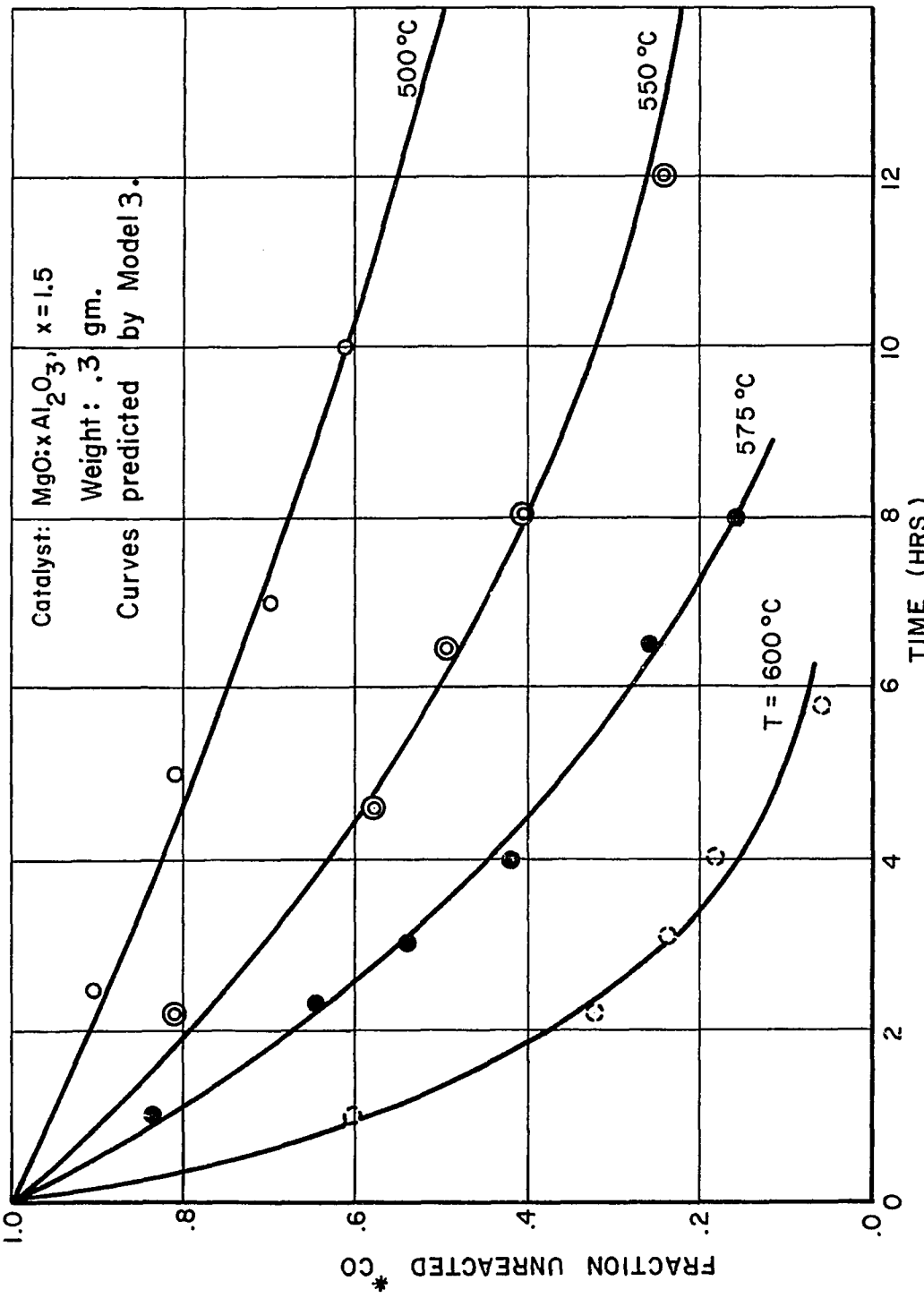

FIGURE II. FRACTION UNREACTED $^{*}CO$ VERSUS TIME.

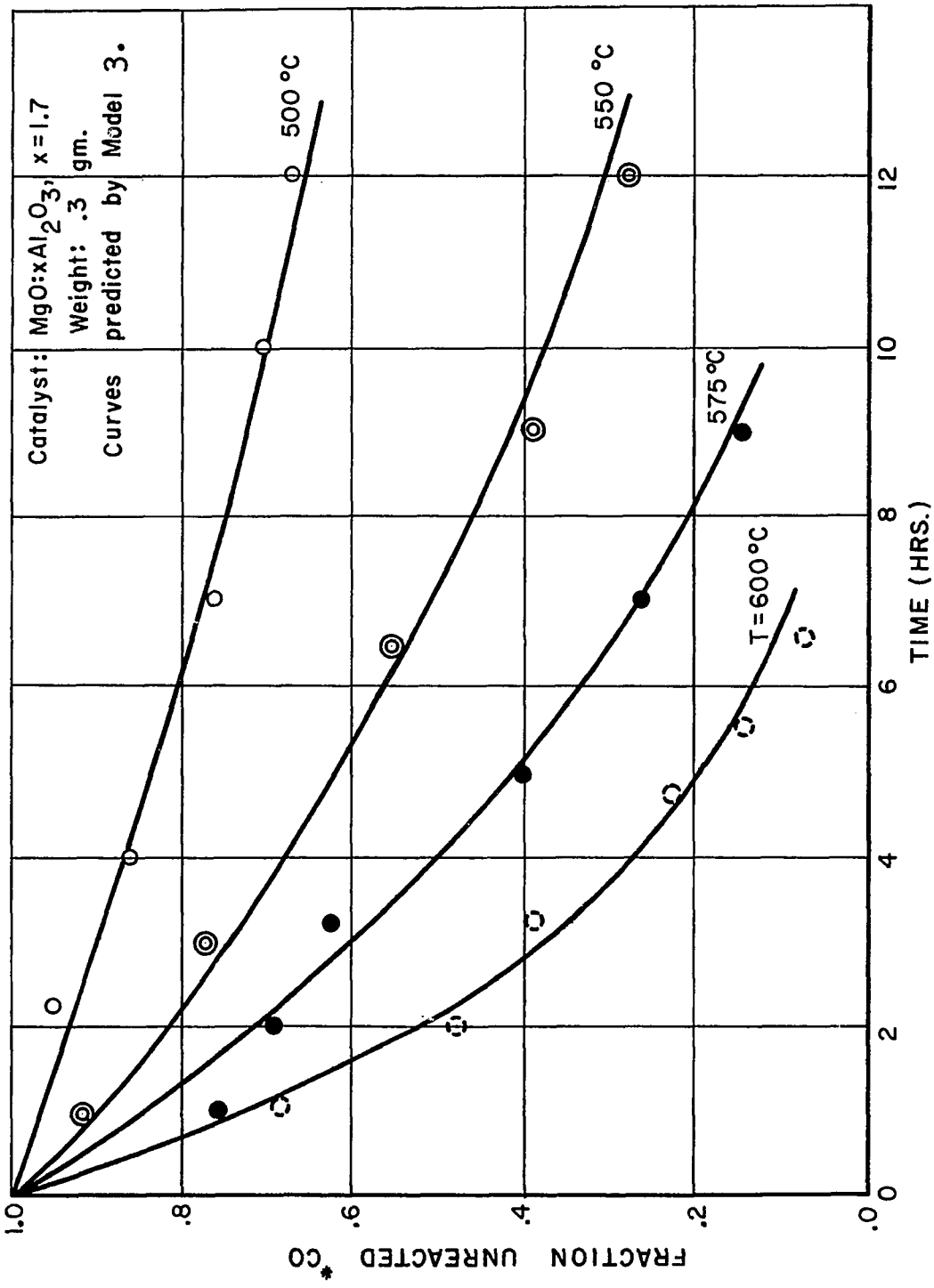

FIGURE 12. FRACTION UNREACTED *CO VERSUS TIME.

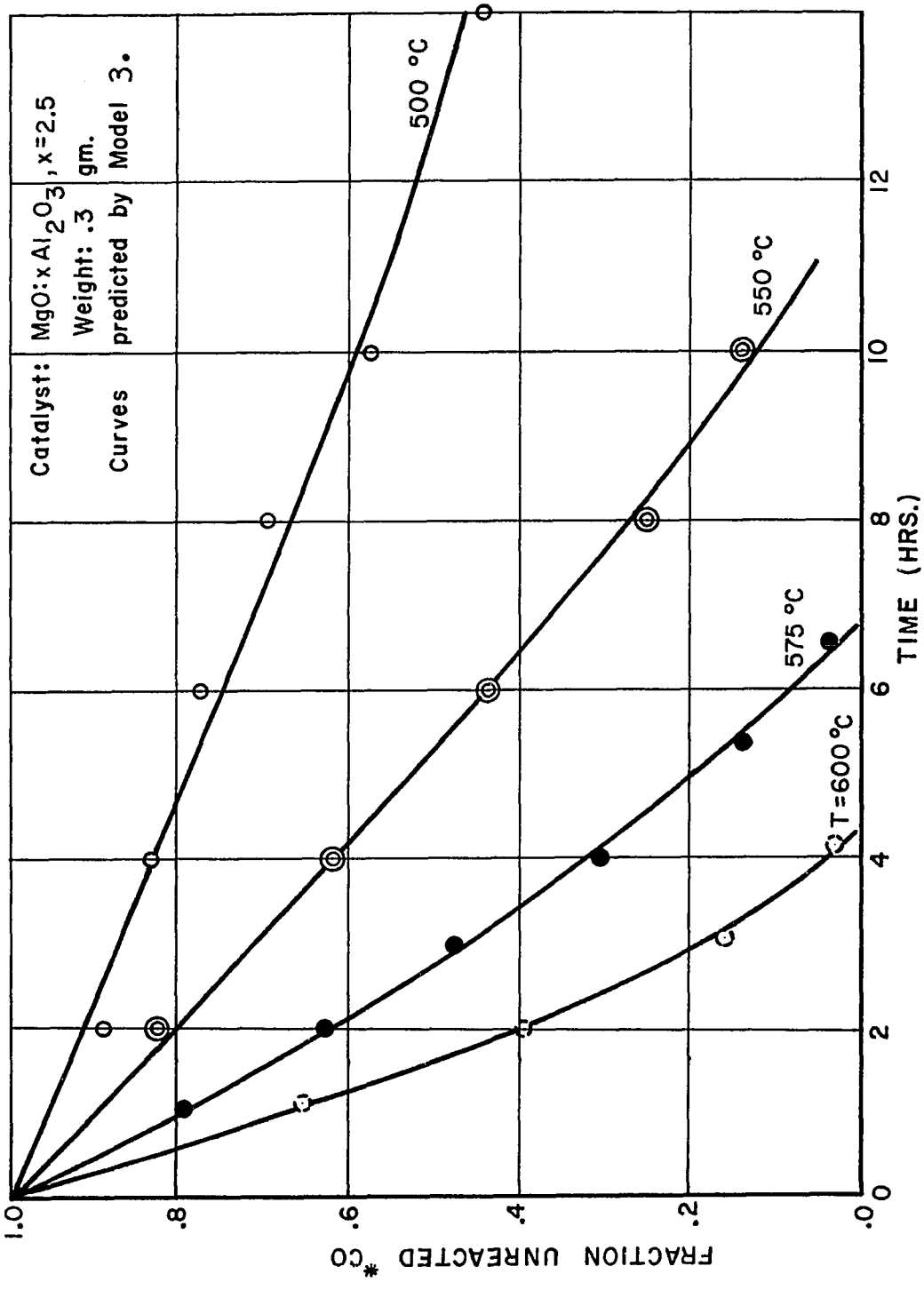

FIGURE 13. FRACTION UNREACTED *CO VERSUS TIME.

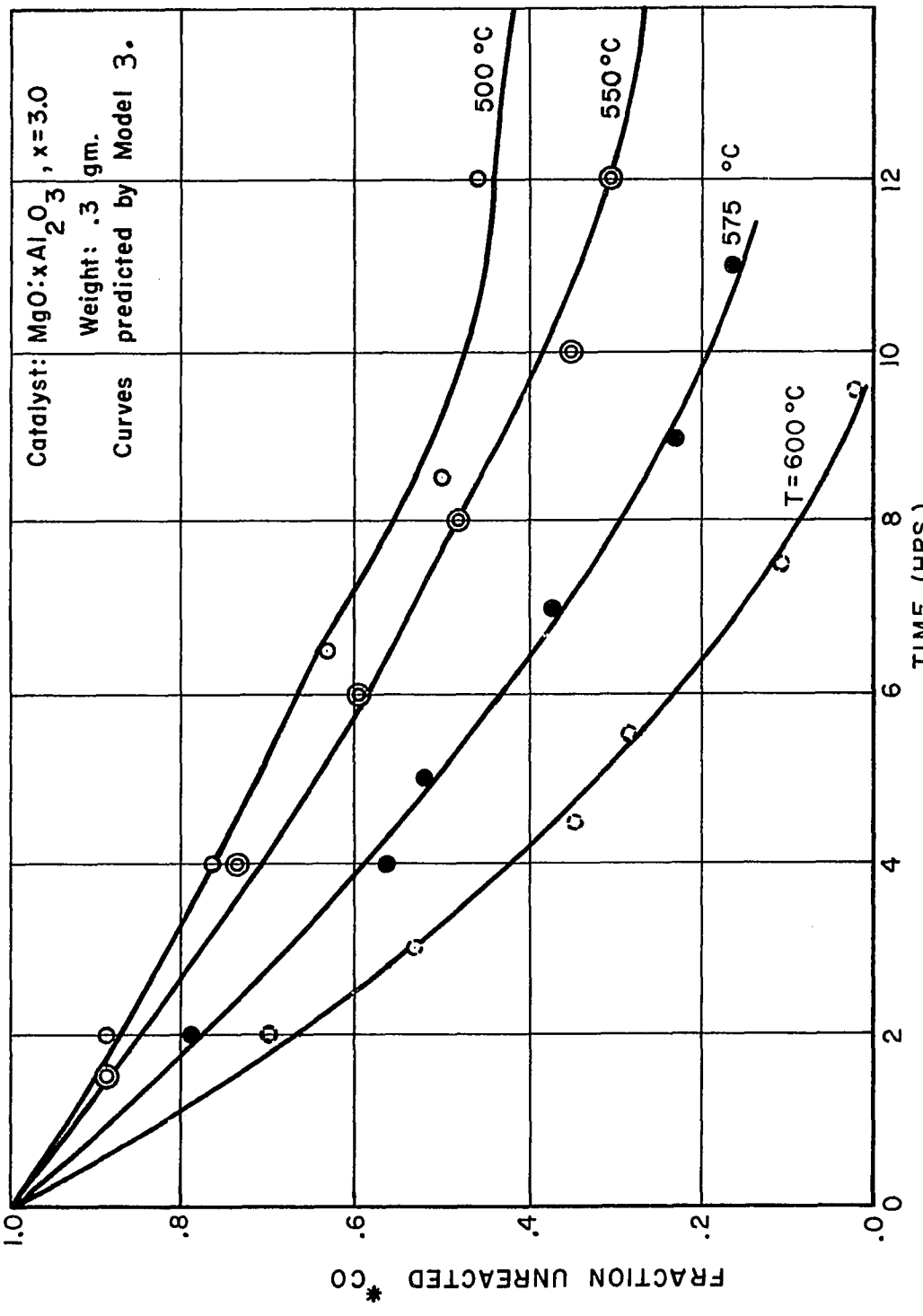

FIGURE 14. FRACTION UNREACTED *CO VERSUS TIME.

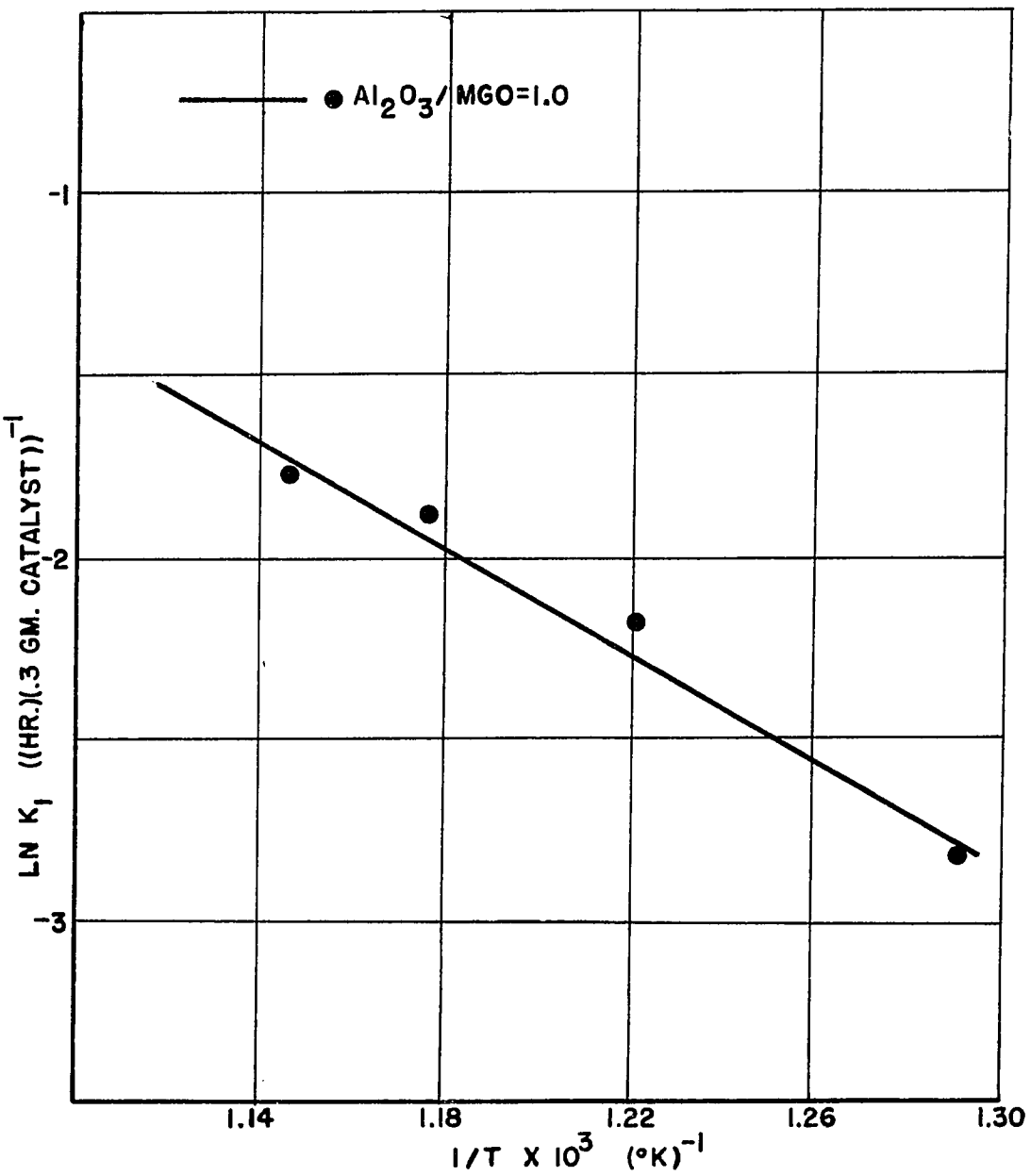

FIGURE 15. ARRHENIUS PLOT: LN K_1 VS. 1/T

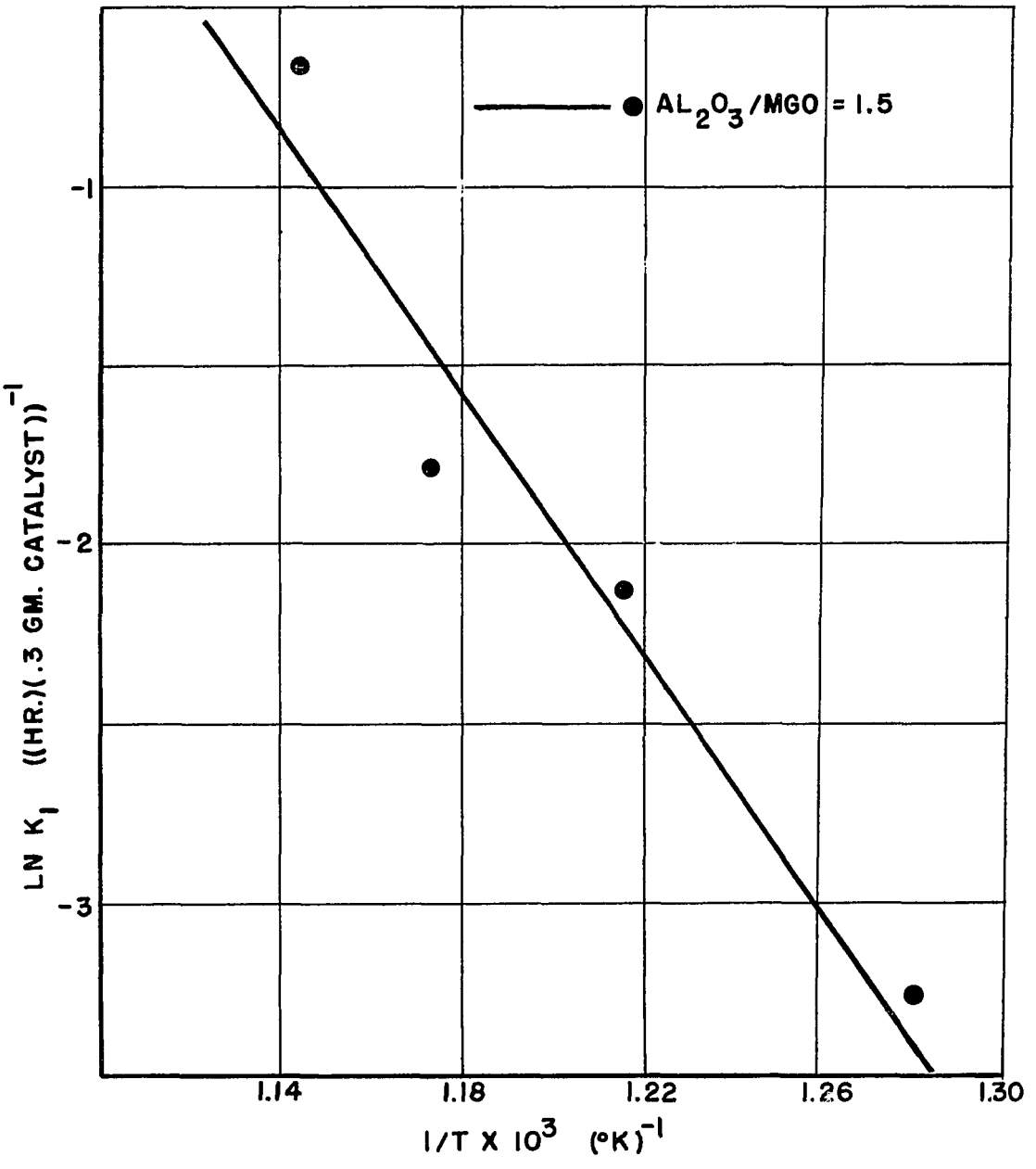

FIGURE 16. ARRHENIUS PLOT: LN K_1 VS. 1/T

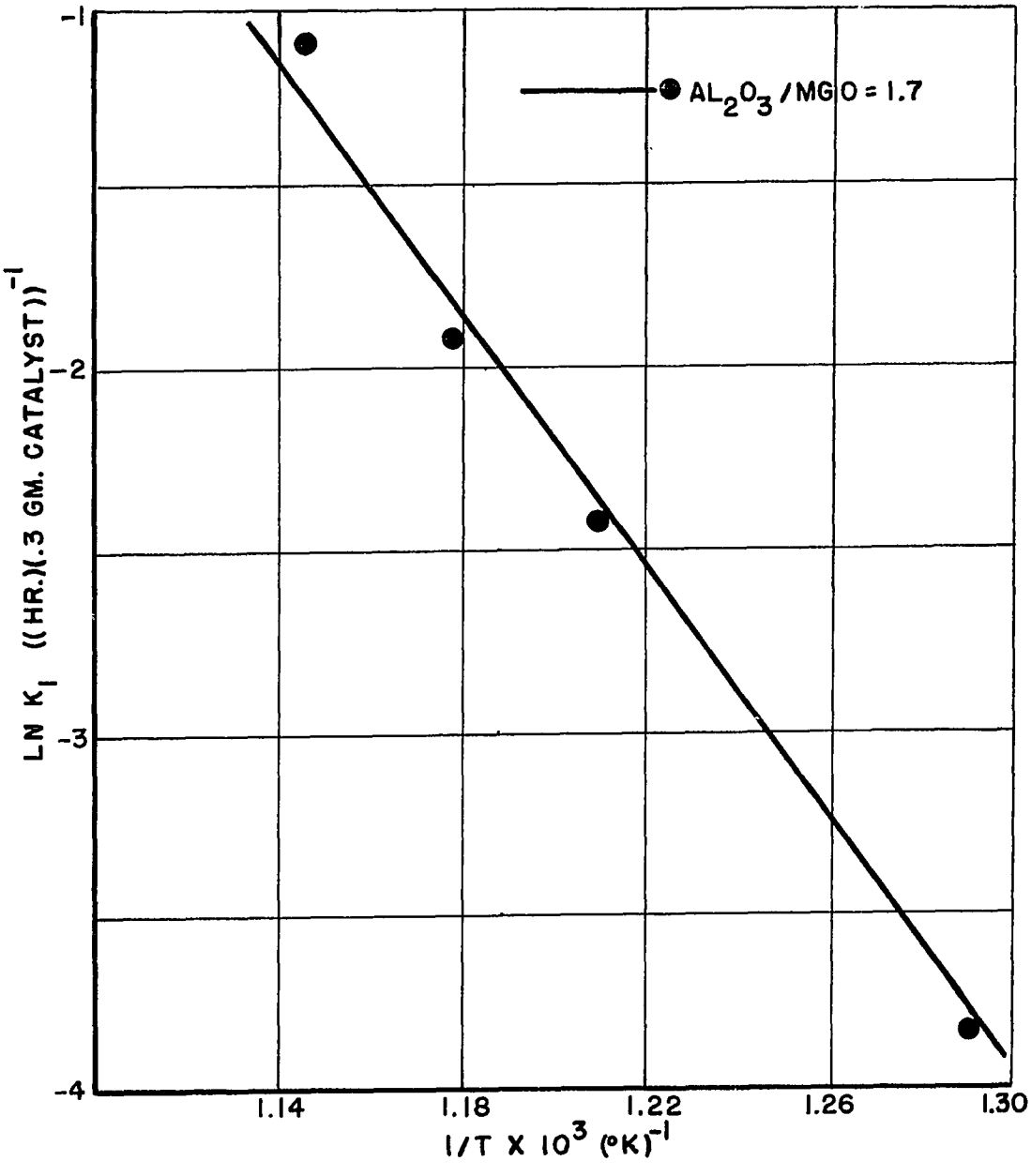

FIGURE 17. ARRHENIUS PLOT: LN K_1 VS. 1/T.

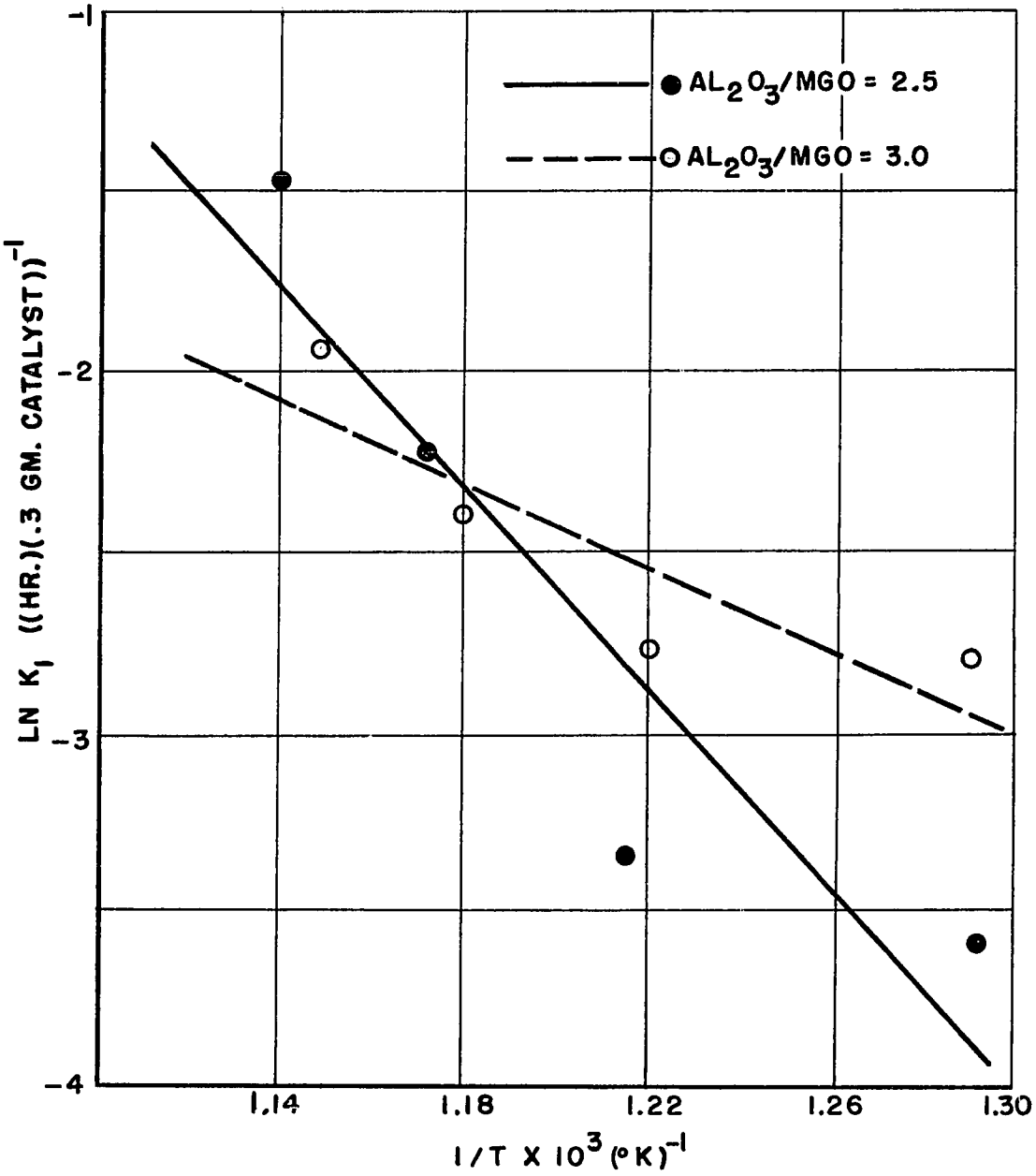

FIGURE 18. ARRHENIUS PLOT: LN K_1 VS. 1/T.

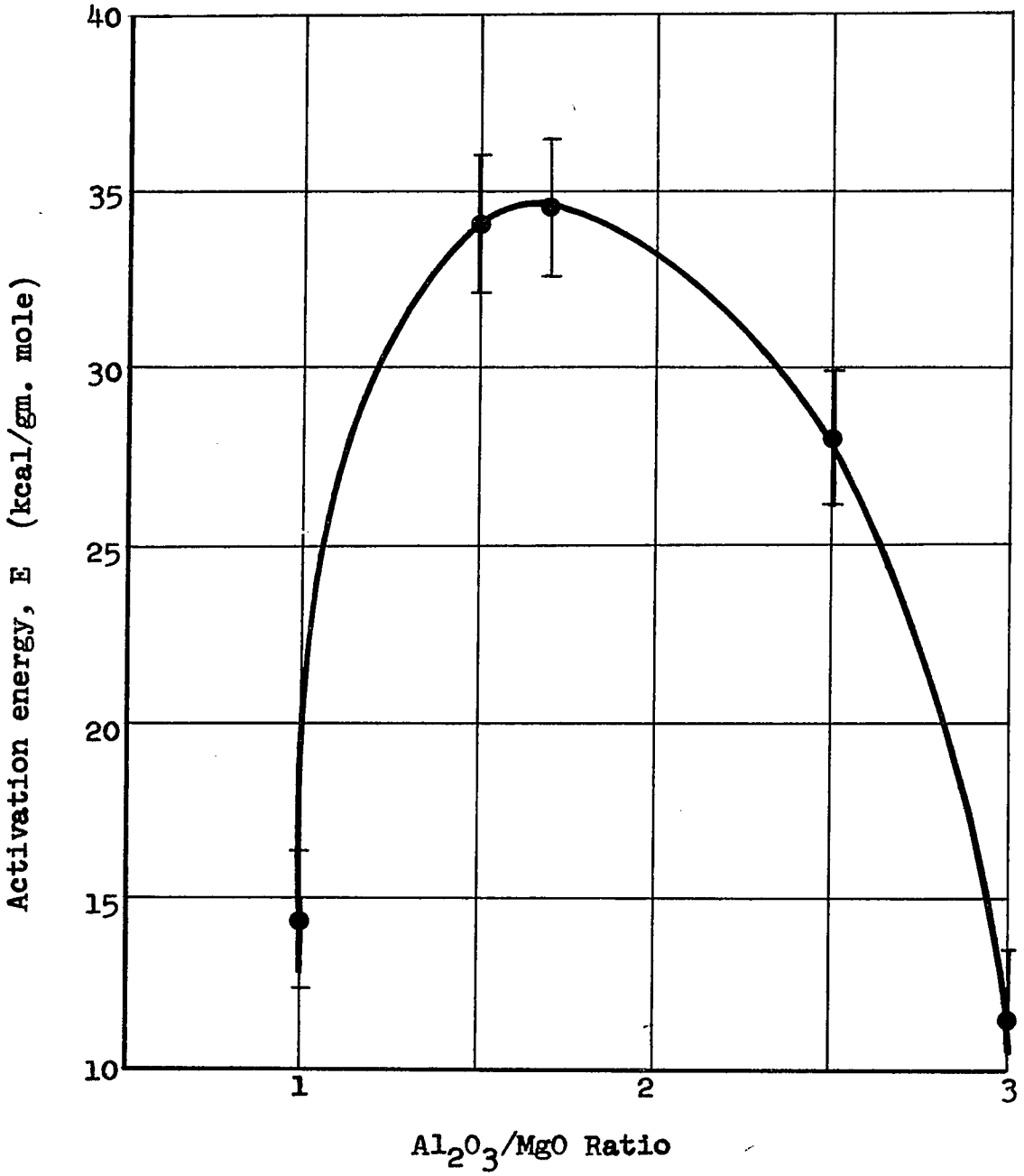

Figure 19. Activation energy, E versus composition of magnesium aluminate.

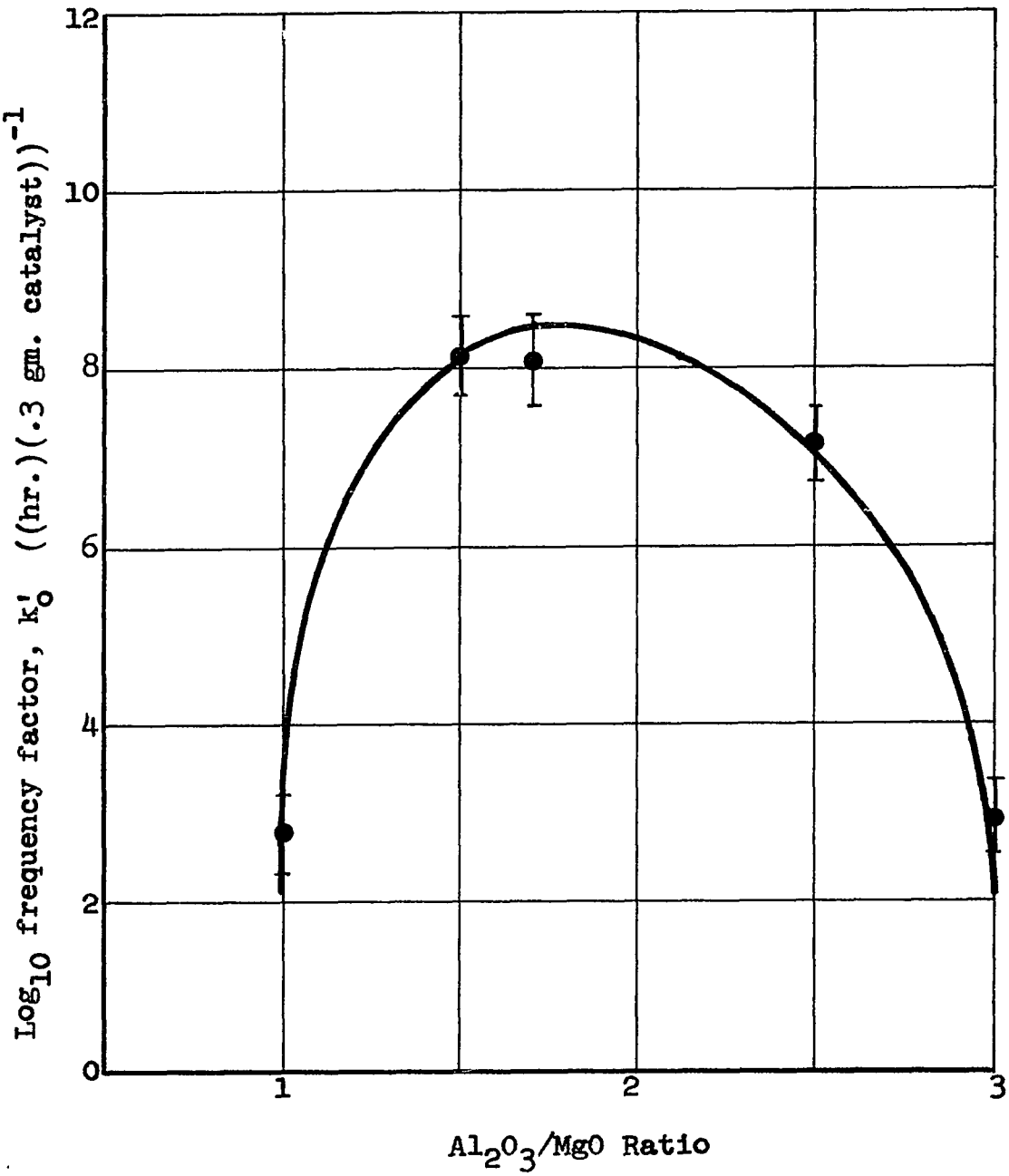

Figure 20. Log_{10} frequency factor, k_o' versus composition of magnesium aluminate.

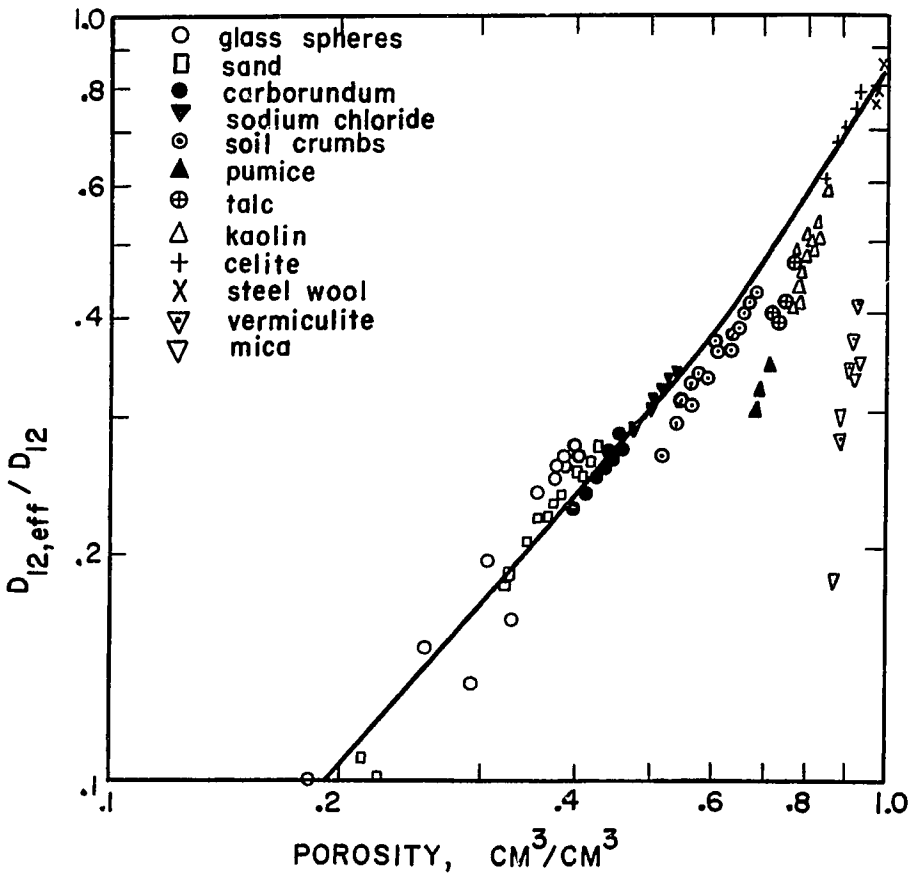

FIGURE 21. HYDROGEN-AIR DIFFUSION IN UNCONSOLIDATED POROUS MEDIA.[82]

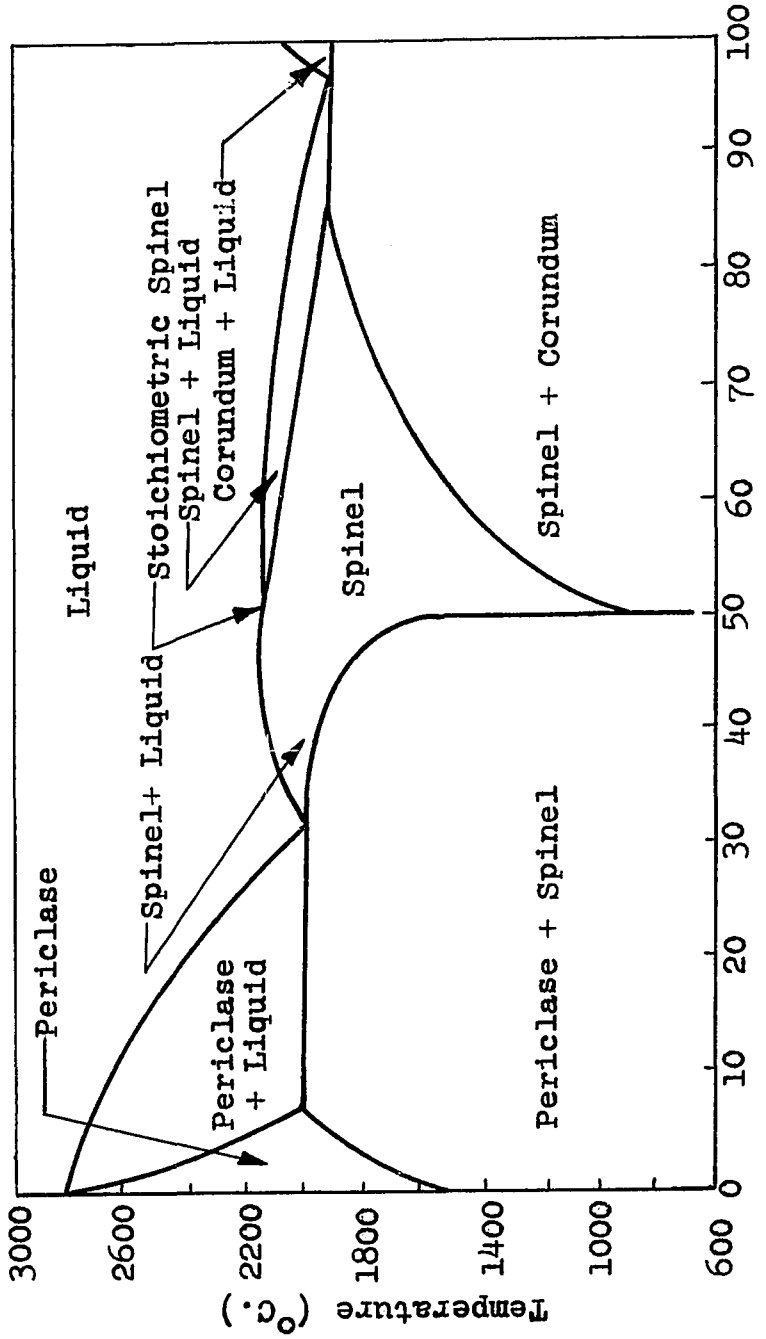

Figure 22. Phase Diagram for the System MgO-Al_2O_3.(85)

REFERENCES

1. De Maio,D.,"Catalyst Selection and Evaluation", Chemical Engineering, 127, July 29, 1968.

2. Thomas,J.M. and Thomas,W.J., Intro. to the Principles of Heterogeneous Catalysis, Academic Press, N.Y. (1967).

3. Ashmore,P.G., Catalysis and Inhibition of Chemical Reactions, Butterworths, London (1963).

4. Wolkenstein,Th., Advances in Catalysis and Related Subjects, 12, 189 (1960).

5. Thomas and Thomas, op. cit., p. 312.

6. Wang,C.C.,"Single Crystal Spinel for Electronic Application", Technical Report AFML-TR-68-320, Air Force Materials Laboratory, Air Force Systems Command, Wright-Patterson Air Force Base, Ohio, October, 1968.

7. Ibid, p. 8.

8. Ibid, p. 50.

9. Ibid, p. 18.

10. Kittel,C. Intro. to Solid State Physics, John Wiley and Sons, Inc., New York (1956,1966).

11. Schwab,G-M. and Block,J.,Z.physik. Chem. N.F., 1, 42 (1954)

12. Hauffe, K., Long, R.G. and Engell, H.J., Z. physik. Chem. 201, 721 (1952).

    Verwey, E J.W., Semiconducting Materials, p. 151, Butterworths, London (1951).

13. Parravano, G.J., Am. Chem. Soc., 75, 1448 (1953)

14. Roginskii, S.Z., Keir, N.P. and Sozonova, I.S., Compt. Rend. U.R.S.S., 106, 859 (1956).

15. Cimino, A., Molinari, E. and Romeo, G., Z. physik. Chem., N.F. 16, 101 (1958).

16. Dry, M.E. and Stone, F.S., Discussions Faraday Soc., 28, 192, (1959).

17. Komatsu, W., Ooki, H., Naka, I. and Kobayashi,A., Journal of Catalysis, 15, 43, (1969).

18. Parravano, G., op. cit., p 1452.

19. Roginskii and Tselinskaya, J. Physic. Chem.Russ.,21 919 (1947); 22, 1360 (1948).

20. Dell, R.M., and Stone, F.S., Trans. Faraday Soc. 50, 501 (1954).

21. Eaton, L.D. and Winter, E.R.S., Journal of Catalysis, 4, 552, (1965).

22. El Shobaky, G., Gravelle, P.C., and Teichner, S.J., Advances in Chemistry Series, American Chemical Soc., Washington, D.C., (1968).

23. El Shobaky, G., Gravelle, P.C., and Teichner, S.J., Journal of Catalysis, 14, 4, (1969).

24. Matsuura, I., Kubokawa, Y. and Toyama, O., J. Chem. Soc. Japan (Pure Chem. Soc.), 81, 997, (1960).

25. Komatsu, W., Ooki, H., Naka, I. and Kobayaxhi, A., Journal of Catalysis, 15, 43, (1969).

26. Schwab, G.M., and Block, J., Z. Physik. Chem,(Frankfurt), (NF), 1, 42 (1954).

27. Wagner, C.J., J. Chem. Phys. 18, 69 (1950).

Hauffe, K., Long, R.G. and Engell, H.J, Z. physik. Chem. 201, 721, (1952).

28. Chon,H. and Prater, C.D., Discussions Faraday Soc. 41, 380, (1966).

29. Amigues, P., and Teichner, S.J., Discussions Faraday Soc., 41, 362, (1966).

30. Sancier, K.M., Journal of Catalysis, 9, 331 (1967).

31. Hoang-Van, C. and Teichner, S.J., Journal of Catalysis, 16, 69, (1970).

32. Stone, F.S., Advan. Catal. Relat. Subj., 13, 1, (1962).

33. Bragg, W.H., Phil. Mag. 6, 305 (1915).

34. Verwey, E. and Heilman, W., J. Chem. Phys 15, 174 (1947)

35. Bacon, G.E., Acta Phys. 30, 24 (1959).

36. Saalfeld, H. and Jagodzinski, H., Z. Krist. 109, 87 (1957).

37. Farrell, E.F., Linz, A., and Redman, M., Contract Report, AF19(628)-3884 (1965).

38. Wang, C.C., op. cit., p. 50.

39. Ibid, p. 8.

40. Ibid, p. 10.

41. Lang, A.R., J. Appl. Phys. 30, 1748 (1959).

42. Wang, C.C., op. cit., p. 18.

43. Ibid, p. 18.

44. Hougen, O.A. and Watson, K.M., Chemical Process Principles, Part III: Kinetics and Catalysis, John Wiley and Sons, Inc., New York (1947).

45. Levenspiel, O., Chemical Reaction Engineering, John Wiley and Sons, Inc., New York (1962).

Smith, J.M., Chemical Engineering Kinetics, McGraw-Hill, New York (1956 , 1970)

46. Advances in Catalysis and Related Subjects. Rideal,E.K. et al, ed., N.Y.: Acamemic Press (1948-1972)
Journal of Catalysis. DeBoer, J.H. and Selwood, P.W., ed., N.Y.: Academic Press (1962-1972)

47. Hougen, O.A., and Watson, K.M., op. cit. p. 943.

48. Chou, Chan-Hui, Industrial and Engineering Chemistry 50, 799, (1958).

49. Blakemore, J.W. and Hoerl, A.E., Chem. Engr. Progr. Symposium Series No. 42, 59, 14 (1963).

50. Kittrell, J.R., Hunter, W.G., and Watson, C.C., A.I.C.H.E. Journal, 11, 1051 (1965)

51. Himmelblau, D.M., Process Analysis by Statistical Methods, John Wiley and Sons, Inc. (1970).

52. Kittrell, J.R., Hunter, W.G. and Watson, C.C.,A.I.C.H.E. Journal 12, 5 (1966); 11, 1051 (1965).

53. Lapidus, L. and Peterson, T.I., A.I.C.H.E. Journal 11, 891, (1965).

54. Draper, N.R. and Smith, H., Applied Regression Analysis, John Wiley and Sons, Inc.,New York (1966).

55. Lapidus L. and Peterson, T.I., op. cit.

56. Shah, M.J. and Davidson, B., Ind. & Eng. Chem. 57(10) 18 (1965).

57. Kittrell, J.R., Hunter, W.G. and Watson, C.C., A.I.C.H.E. Journal 12, 5 (1966); 11, 1051 (1965).

Kittrell, J.R., Mezaki, R. and Watson, C,C., Ind. & Eng. Chem. 57(12), 18, (1965).

58. Lapidus, L. and Bard, Y., Catalysis Reviews 2(1), 67 (1968).

59. Lapidus, L. and Peterson, T.I., Share Program 7090 T2 IBM 0014 (1964).

60. Wilde, D.J. and Beightler, C.S., Foundations of Optimization, Prentice-Hall, Inc., Englewood Cliffs, N.J. (1967).

61. Eisenpress, H., Bomberault, A. and Greenstadt J., IBM 7090, Share Program 7090 IBM 0035 (1966).

62. Bard, Y., Nonlinear Parameter Estimation and Programming, Program 360D 13.6.003, IBM, Hawthorne,N.Y.

63. Lapidus, L. and Bard, Y., op. cit., p. 84.

64. Davidson, W.C., A.E.C. Res.Develop. Rept. ANL-5990 (1959).

65. Marquardt, D.W., Share Program No. 3094 (1963).

66. Marquardt, D.W., J. Siam, 11 431 (1963).

67. Levenspiel, O., op. cit.

68. Garner, W.E., Advan. Catalysis and Related Subj. 9, 169, (1952).

69. Balandin, A.A., Catalysis and Chemical Kinetics, Academic Press, New York (1964).

70. Wagner, C. and Hauffe, K., Z. Elektrochem. 44, 172, (1938).

71. Parravano G., J. Am. Chem. Soc. 75, 1448, (1953).

72. Lewis, B. and Von Elbe, G., Combustion, Flames and Explosions of Gases, Academic Press, New York (1961).

73. El Shobaky, G., Gravelle, P.C. and Teichner, S.J., Advances in Chemistry Series, American Chemical Soc., Washington, D.C. (1968).

74. Amigues, P. and Teichner, S.J., op. cit., p.406.

75. Semenoff, N., Chemical Kinetics and Chain Reactions, Oxford at the Clarendon Press, London (1935).

76. Dixon, W.J. and Massey, F.J., Introduction to Statistical Analysis, McGraw-Hill Book Co., N.Y. (1969).

77. Claudel, B.M. and Brau, G.G., Journal of Catalysis, 14, 322 (1969).

78. Bond, G.C., Catalysis by Metals, Academic Press, New York (1962).

79. Wang, C.C., private communication, David Sarnoff Research Center (RCA), Princeton, N.J. (1970).

80. Christman, D.R. and Wolf, A.P., Analytical Chemistry, 27, 1940 (1955).

81. Ibid., p. 1940.

82. Satterfield, C.N. and Sherwood, T.K., The Role of Diffusion in Catalysis, Addison Wesley, Reading, Mass. (1963)

83. Ibid. p. 15.

84. Ibid. p. 62.

85. Alper et al, J. Am. Ceram Soc., 45, 263 (1962).

86. Balandin, A.A., Z. phys. Chem., 132, 289 (1929).

87. Emmett, Paul H., New Approaches to the Study of Catalysis, Pennslyvania State Univ., University Park, Pa. (1962).

88. Christian, J.W., The Theory of Transformations in Metals and Alloys, Pergamon Press, New York (1965).

89. Grabmaier, J.G. and Galckenberg, H.R., J. Am. Cer. Soc., 52, 648 (1969)

90. Cahn, R.W., Physical Metallurgy, John Wiley & Sons, Inc., New York (1965).

91. Mehl, R.F. and Jetter, L.K., Age Hardening of Metals Symposium of the American Society for Metals, p.342 (1939).

92. Kelly, A. and Nicholson, R.B., Progress in Materials Science, 10, 151 (1963).

93. Richman, Marc H., An Introduction to the Science of Metals, Blaisdell Pub. Co., p. 317 (1967).

94. Garner, W.E., Gray, T.J. and Stone, F.S., Proc. Roy. Soc., A197, 294 and 314 (1949)

95. Draper, N.R. and Smith, H., Applied Regression Analysis, John Wiley & Sons, Inc., New York (1966)

96. Huang, Ching-Rong, Oxygen Transfer at Cobalt Ferrite Surface, Ph.D. Dissertation, The University of Michigan, Ann Arbor, Michigan (1966).

Squires, R.G., private communication, Purdue University, Lafayette, Indiana (1970).

VITA

Name: James A. Whelan

College	Dates	Degrees	Date of degree
Union College (N.J.)	1962-64	A.A.	1964
N.C.E.	1964-66	B.S.Ch.E.	1966
N.C.E.	1966-68	M.S.Ch.E.	1968

Positions held:

1970-1971	Christian Brothers College, 650 East Parkway South, Memphis, Tenn. Assistant Professor in Chemical Engr.
1969-1970	Newark College of Engineering, Newark,N.J. N.D.E.A. Fellowship. Doctoral student.
1966-1969	Newark College of Engineering, Newark,N.J. Teaching Fellow. Masters-Doctoral student.
Summers 1967-1968	Veteran's Administration Hospital, East Orange, N.J. Research Assistant.
Summer 1966	Eastman Kodak Company, Rochester, N.Y. Development Engineer.
Summer 1965	Eclipse Pioneer Div., Bendix Aviation Corp., Teterboro, N.J. Draftsman.
Summers 1963-1964	Vector Engineering, Inc., Springfield, N.J. Draftsman.
1/62-7/62	Summit Engineers, Inc., 409 Broad St., Summit, N.J. Draftsman.
7/6--12/61	Automatic Switch Co., Hanover Rd., Florham Park, N.J. Draftsman.